

Clusterpath Gaussian Graphical Modeling

Daniel J.W. Touw¹, Andreas Alfons¹, Patrick J.F. Groenen¹, and Ines Wilms²

¹Department of Econometrics, Erasmus University Rotterdam

²Department of Quantitative Economics, Maastricht University

Abstract

Graphical models serve as effective tools for visualizing conditional dependencies between variables. However, as the number of variables grows, interpretation becomes increasingly difficult, and estimation uncertainty increases due to the large number of parameters relative to the number of observations. To address these challenges, we introduce the *Clusterpath estimator of the Gaussian Graphical Model* (CGGM) that encourages variable clustering in the graphical model in a data-driven way. Through the use of a clusterpath penalty, we group variables together, which in turn results in a block-structured precision matrix whose block structure remains preserved in the covariance matrix. We present a computationally efficient implementation of the CGGM estimator by using a cyclic block coordinate descent algorithm. In simulations, we show that CGGM not only matches, but oftentimes outperforms other state-of-the-art methods for variable clustering in graphical models. We also demonstrate CGGM's practical advantages and versatility on a diverse collection of empirical applications.

Keywords: clusterpath, graphical modeling, hierarchical clustering, precision matrix, unsupervised learning

1 Introduction

Gaussian graphical models (GGM) have become an increasingly popular tool for summarizing conditional dependencies among a set of p variables. In particular, a GGM is a conditional dependency network where one refers to the p variables in the graphical model as the *nodes* and the *edges* represent the conditional dependency relations among each pair of variables. Estimating GGMs is statistically challenging when the number of parameters $(p(p+1)/2)$ is large relative to the number of observations (n), leading to large variability in estimation. Yet, such a setting arises across many and diverse scientific areas, ranging from, amongst others, gene regulatory networks in biology to contagion networks in finance and brain activation networks in neuroscience. This has led to a flourishing area on regularized estimation methods for GGMs (e.g.,

Meinshausen & Bühlmann, 2006; Peng et al., 2009; Yuan, 2010; Cai et al., 2011) that impose simplifying structures on the estimated parameters. While much of the existing literature focuses on reducing the estimation variability through edge sparsity, our approach branches into a different direction by using node aggregation. Specifically, we integrate convex clustering into the GGM framework to reduce estimation variability through the pooling of estimates for similar variables.

Edge sparsity in GGMs through, for instance, ℓ_1 -regularization has long formed the predominant choice to reduce dimensionality in GGMs (e.g., Yuan & Lin, 2007; Banerjee et al., 2008; Friedman et al., 2008; Rothman et al., 2008). The focus here is to sparsely estimate the precision matrix (i.e., the inverse of the covariance matrix) since conditional independencies between variable-pairs can be directly obtained from its sparsity patterns, or equivalently the absence of edges in the estimated GGM, offering an appealing interpretability advantage. Several recent studies, however, point to a number of important drawbacks when solely relying on edge sparsity as simplifying structure. First, when the number of nodes grows large compared to a small sample size, conditional dependencies among the variables may become too weak to detect (Eisenach et al., 2020). Such a situation is nowadays likely to occur more frequently since (often noisy) data across many scientific areas are measured at higher resolutions (Wilms & Bien, 2022). Second, sparsely estimated GGMs with many variables may still contain a large number of edges, thereby hindering interpretability (Grechkin et al., 2015). Third, many real world networks exhibit more complex structures than mere edge sparsity implies. For instance, it is not the most suitable simplicity structure for networks containing hub nodes, that is, a group of nodes with similar and often strong dependency structures (Hosseini & Lee, 2016; Tarzanagh & Michailidis, 2018; Tarzanagh et al., 2021), or bipartite structures where some variables depend linearly on others (Heinävaara et al., 2016).

When GGMs face such challenges, one is often not interested in estimating conditional dependencies among the many observed variables but instead among a smaller number of (unobserved) *clusters* (also called communities) of original variables that share the same behavior. For instance, biologists estimate large-scale gene regulatory networks and cluster genes into pathways to unravel dependencies among them (e.g., Marlin & Murphy, 2009; Grechkin et al., 2015; Kumar et al., 2020), neuroscientists analyzing fMRI data routinely cluster voxels into regions of interest to learn interaction networks of brain activation (e.g., Pircalabelu & Claeskens, 2020), financial analysts may cluster company stocks into industry sectors to study how shocks can spread over the market by contagion (e.g., Cardoso et al., 2020). Cluster analysis is one of the most popular unsupervised learning methods to discover the underlying group structures in data. Variable clustering in the context of GGMs not only offers simple, interpretable dependency networks but may also boost the dependency signals (Eisenach et al., 2020).

To estimate GGMs with clustered variables, a recent yet growing interest arose in *node-based* dimensionality reduction. Initial proposals assume the clusters to be known *a priori* and incorporate this information in

the regularization framework to encourage within-cluster dependencies over cross-cluster dependencies (e.g., Duchi et al., 2008; Schmidt et al., 2009). Subsequent works learn the node clustering either by decoupling the clustering task from the estimation of the GGM (e.g., Ambroise et al., 2009; Marlin & Murphy, 2009; Tan et al., 2015; Eisenach et al., 2020; Brownlees et al., 2022; Shi et al., 2024) or by simultaneously conducting both tasks (e.g., Hosseini & Lee, 2016; Nie et al., 2016; Tarzanagh & Michailidis, 2018; Kumar et al., 2020; Pircalabelu & Claeskens, 2020; Wilms & Bien, 2022). Yet, to the best of our knowledge, the potential to leverage penalty structures popular in the literature on convex clustering (Pelckmans et al., 2005; Hocking et al., 2011; Lindsten et al., 2011) to combine node clustering jointly with the estimation of the GGM is left largely unexplored, a notable exception being Yao & Allen (2019) which we further contrast to our proposal in Section 2.4.

In this paper, we develop a novel regularizer, called the *Clusterpath estimator of the Gaussian Graphical Model*, *CGGM* in short, to estimate GGMs that are node-clustered where neither the number of clusters nor their composition needs to be known in advance. To this end, we propose a novel penalty on the distances between the variables in the precision matrix and embed this in a convex optimization framework for which we offer a computationally efficient cyclic block coordinate descent algorithm. The resulting estimated precision matrix has a block structure where all variables belonging to the same cluster share the same within- as well as cross-cluster dependencies. A unique property of our approach for clustering the precision matrix is that its inverse retains the same block structure, a property not shared by other approaches.

We evaluate the performance of CGGM against state-of-the-art methods for estimating node-clustered GGMs through a comprehensive simulation study covering a wide range of graph structures. Our results indicate that CGGM frequently surpasses the benchmark methods in both estimation accuracy and clustering performance. CGGM performs competitively in scenarios with clear sparsity patterns, even without a dedicated sparsity-inducing penalty. While the main focus of our study is on estimating clustered precision matrices to create graphical models, we also demonstrate that CGGM can be easily extended to estimate clustered covariance matrices. In fact, when a block structure in the covariance matrix (instead of the precision matrix) is the object of interest, we demonstrate that directly estimating a clustered covariance matrix has practical advantages over inverting a clustered precision matrix estimate, even though the latter also yields a block structure in the covariance matrix. Finally, we illustrate the effectiveness and versatility of CGGM on three practical applications involving (i) stock market data from the S&P 100, (ii) OECD well-being indicators, and (iii) survey data on participants’ humor styles.

The remainder of the paper is organized as follows. Section 2 introduces the clusterpath estimator for GGMs, details the cyclic block coordinate descent algorithm, and relates our proposal to existing work. Next, we describe the simulation study and present its results in Section 3. Section 4 explores the use of CGGM

for directly estimating clustered covariance matrices instead of precision matrices. Section 5 demonstrates the application of CGGM to empirical data, and Section 6 concludes the paper.

2 The Clusterpath Estimator for the Gaussian Graphical Model

We begin in Section 2.1 by discussing GGMs with clustered variables, followed by the introduction to the clusterpath estimator in Section 2.2. Section 2.3 details the cyclic block coordinate descent algorithm used to compute our estimator. Finally, Section 2.4 relates our proposal to existing work.

2.1 Clustered Gaussian Graphical Models

Let \mathbf{X} be an $n \times p$ matrix of n multivariate normal observations each of dimension p , with sample mean \mathbf{m} and sample covariance matrix \mathbf{S} . Denoting the population covariance matrix by $\mathbf{\Sigma}$, our target of estimation is the precision matrix $\mathbf{\Theta} = \mathbf{\Sigma}^{-1}$. Under the assumption of a multivariate normal distribution, the precision matrix can be equivalently expressed in a graph where the nodes represent the p variables and the edge weights are given by the entries in $\mathbf{\Theta}$ which represent the conditional dependencies among the variables.

Our goal is to estimate the precision matrix $\mathbf{\Theta}$ (and hence the graph structure of the GGM) by encouraging clustering of the p nodes in the graph. The K new cluster variables ξ_1, \dots, ξ_K then represent the average of the variables that belong to that cluster, with K typically much smaller than p to achieve dimensionality reduction in the parameters defining $\mathbf{\Theta}$. The edge weights among the clustered variables represent the conditional dependencies among the K new cluster variables. Clustering of the variables in the graph corresponds to a block structure in the rows and columns of $\mathbf{\Theta}$, see the so-called *G-block* format introduced in Bunea et al. (2020) and discussed by Wilms & Bien (2022) in the context of GGMs. The block-structure of the precision matrix can then be written as

$$\mathbf{\Theta} = \begin{bmatrix} (a_{11} - r_{11})\mathbf{I} & \mathbf{0} & \dots & \mathbf{0} \\ \mathbf{0} & (a_{22} - r_{22})\mathbf{I} & \dots & \mathbf{0} \\ \vdots & \vdots & \ddots & \vdots \\ \mathbf{0} & \mathbf{0} & \dots & (a_{KK} - r_{KK})\mathbf{I} \end{bmatrix} + \begin{bmatrix} r_{11}\mathbf{1}\mathbf{1}^\top & r_{12}\mathbf{1}\mathbf{1}^\top & \dots & r_{1K}\mathbf{1}\mathbf{1}^\top \\ r_{21}\mathbf{1}\mathbf{1}^\top & r_{22}\mathbf{1}\mathbf{1}^\top & \dots & r_{2K}\mathbf{1}\mathbf{1}^\top \\ \vdots & \vdots & \ddots & \vdots \\ r_{K1}\mathbf{1}\mathbf{1}^\top & r_{K2}\mathbf{1}\mathbf{1}^\top & \dots & r_{KK}\mathbf{1}\mathbf{1}^\top \end{bmatrix}, \quad (1)$$

where $\mathbf{A} = \text{diag}(a_{11}, \dots, a_{KK})$ is a $K \times K$ diagonal matrix, $\mathbf{R} = (r_{k\ell})_{1 \leq k, \ell \leq K}$ is a $K \times K$ symmetric matrix, and \mathbf{I} is the identity matrix of appropriate dimension, similarly for $\mathbf{1}$ denoting a column-vector of ones and for $\mathbf{0}$ denoting a matrix of zeros. The within-cluster conditional variances a_{kk} and covariances r_{kk} are the same for all p_k variables within cluster k . These p_k variables in cluster k also have the same conditional covariance $r_{k\ell}$ with all p_ℓ variables belonging to another cluster ℓ . This clustered GGM is visualized for a toy example with $p = 8$ variables and $K = 3$ clusters in Figure 1.

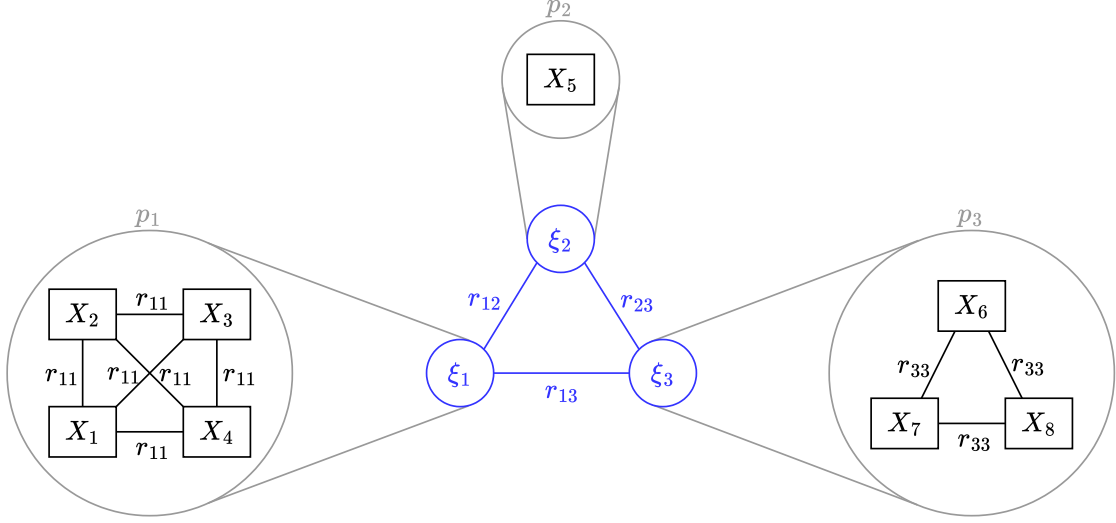


Figure 1: Toy example of a graph representing the clustered precision matrix with $K = 3$ clusters constructed from $p = 8$ original variables. Cluster variable ξ_1 is the average of the $p_1 = 4$ variables X_1, X_2, X_3 , and X_4 having within cluster conditional covariance r_{11} . Cluster variable ξ_2 is a singleton ($p_2 = 1$) and equal to the original variable X_5 . Cluster variable ξ_3 is the average of the $p_3 = 3$ variables X_6, X_7 , and X_8 having within cluster conditional covariance r_{33} . The three cluster variables have conditional covariances r_{12}, r_{13} , and r_{23} .

An important implication of our assumed block structure that is not shared by other approaches is that the clustering structure of Θ is retained when taking the inverse (see, e.g., Gower & Groenen, 1991; Archakov & Hansen, 2022). This property is lost in the approaches proposed by Yao & Allen (2019), Pircalabelu & Claeskens (2020), and Wilms & Bien (2022). Section 4 explores the estimation of block-structured covariance matrices using CGGM through a numerical experiment.

2.2 Clusterpath Estimator

To estimate precision matrices with a block structure corresponding to clustered variables, we use a convex penalization method of the form

$$\hat{\Theta} = \underset{\Theta}{\operatorname{argmin}} L(\Theta) \quad \text{s.t. } \Theta = \Theta^\top, \Theta \succ 0, \quad (2)$$

$$L(\Theta) = -\log |\Theta| + \operatorname{tr} \mathbf{S}\Theta + \lambda \mathcal{P}(\Theta), \quad (3)$$

where $\log |\cdot|$ denotes the logarithm of the determinant, $\operatorname{tr}(\cdot)$ is the trace, $\cdot \succ 0$ denotes a positive definite matrix, $\lambda \geq 0$ is a tuning parameter controlling the degree of penalization, and $\mathcal{P}(\Theta)$ is the convex clusterpath

penalty penalizing differences between columns $\boldsymbol{\theta}_j$ and $\boldsymbol{\theta}_{j'}$ of the precision matrix $\boldsymbol{\Theta}$. We take

$$\mathcal{P}(\boldsymbol{\Theta}) = \sum_{j < j'} w_{jj'} d_{jj'}(\boldsymbol{\Theta}) \quad \text{with} \quad d_{jj'}(\boldsymbol{\Theta}) = \sqrt{(\theta_{jj} - \theta_{j'j'})^2 + \sum_{\substack{m=1 \\ m \notin \{j, j'\}}^P (\theta_{jm} - \theta_{j'm})^2},$$

and weights $w_{jj'}$ for every pair $1 \leq j, j' \leq p$. These weights determine the fundamental attraction between two variables and are specified beforehand based on, for example, domain knowledge or the pairwise distances based on the sample precision matrix \mathbf{S}^{-1} . We further discuss the choice of weights in Section 2.3.

The objective function is convex since each of the terms in (3) is convex in $\boldsymbol{\Theta}$ and $\boldsymbol{\Theta}$ lies in the convex cone of positive definite matrices. For $\lambda = 0$, one obtains the inverse of the sample covariance matrix as estimate, hence there is no block structure in the precision matrix, nor a clustering of nodes in the GGM. If $d_{jj'}(\boldsymbol{\Theta}) = 0$ and λ is positive, then two vectors $\boldsymbol{\theta}_j$ and $\boldsymbol{\theta}_{j'}$ have exactly the same elements while ignoring $\theta_{jj'}$ and $\theta_{j'j}$. Note that the distance $d_{jj'}(\boldsymbol{\Theta})$ disregards the difference between $\theta_{jj'}$ and $\theta_{j'j}$ as these are identical due to the symmetry of $\boldsymbol{\Theta}$. The penalty term $d_{jj'}(\boldsymbol{\Theta})$ can thus be interpreted as a group lasso penalty (Yuan & Lin, 2006), where each pair of variables $j < j'$ forms a group whose elements are the differences between the corresponding entries in the columns $\boldsymbol{\theta}_j$ and $\boldsymbol{\theta}_{j'}$ of the precision matrix. If all respective differences are put to zero, the estimated entries are identical, which in turn effectively blocks columns j and j' in the precision matrix, or equivalently clusters nodes j and j' in the GGM. As λ increases, estimated GGMs are obtained in which more and more variables are clustered, thereby resulting in a *clusterpath* from the p original nodes (no clustering) until one clustered node (full clustering) in the GGM.

The notion of applying a distance-based penalty to pairs of objects stems from convex clustering (Hocking et al., 2011; Lindsten et al., 2011; Pelckmans et al., 2005). In convex clustering, a copy of the data matrix is estimated while penalizing the distances between the rows, thereby facilitating the clustering of observations. Building upon this framework, convex biclustering (Chi et al., 2017) extends the conventional model by introducing a penalty on the distances between columns, which allows for the clustering of variables as well. The alternative provided by clustering variables using the precision matrix offers insights into the underlying probabilistic dependencies within the data.

Next, we re-express the objective function $L(\boldsymbol{\Theta})$ in terms of \mathbf{A} and \mathbf{R} (thereby assuming $1 \leq K \leq p$ clusters) instead of $\boldsymbol{\Theta}$ to permit more efficient expressions and updates for solving optimization problem (2). To this end, we start by re-writing equation (1) as

$$\boldsymbol{\Theta} = \mathbf{U}\mathbf{R}^*\mathbf{U}^\top + \begin{bmatrix} (a_{11} - r_{11})\mathbf{J}_1 & \mathbf{0} & \cdots & \mathbf{0} \\ \mathbf{0} & (a_{22} - r_{22})\mathbf{J}_2 & \cdots & \mathbf{0} \\ \vdots & \vdots & \ddots & \vdots \\ \mathbf{0} & \mathbf{0} & \cdots & (a_{KK} - r_{KK})\mathbf{J}_K \end{bmatrix}, \quad (4)$$

where \mathbf{U} is the $p \times K$ cluster membership matrix with $u_{jk} = 1$ if variable j belongs to cluster k and zero otherwise, $\mathbf{R}^* = \mathbf{R} + \text{diag}((a_{11} - r_{11})/p_1, \dots, (a_{KK} - r_{KK})/p_K)$, and \mathbf{J}_k is the $p_k \times p_k$ centering matrix. Now, equation (4) presents an orthogonal decomposition where the precision matrix is split in two parts, the first part is a linear space that depends on \mathbf{A} and all elements of \mathbf{R} , the second part is an orthogonal linear space that only depends on the diagonal blocks of the precision matrix, namely \mathbf{A} and the diagonal elements of \mathbf{R} .

Using decomposition (4), we can equivalently express the objective function in (3) as

$$\begin{aligned} L(\Theta) &= L(\mathbf{A}, \mathbf{R}) \\ &= -\log |\mathbf{P}^{1/2} \mathbf{R}^* \mathbf{P}^{1/2}| - \sum_{k=1}^K (p_k - 1) \log(a_{kk} - r_{kk}) + \text{tr} \mathbf{S} \mathbf{U} \mathbf{R} \mathbf{U}^\top + \sum_{\ell=1}^K (a_{\ell\ell} - r_{\ell\ell}) \text{tr} \mathbf{S}_\ell + \lambda \mathcal{P}(\mathbf{A}, \mathbf{R}), \end{aligned} \quad (5)$$

where the diagonal matrix $\mathbf{P} = \mathbf{U}^\top \mathbf{U} = \text{diag}(p_1, \dots, p_K)$ contains the number of variables p_k per cluster on the diagonal, $\mathbf{P}^{1/2}$ simply contains their square roots, \mathbf{S}_ℓ is the sample covariance matrix computed from the p_ℓ variables in cluster ℓ , and the clusterpath penalty is reformulated as

$$\mathcal{P}(\mathbf{A}, \mathbf{R}) = \sum_{k < \ell} \mathbf{u}_k^\top \mathbf{W} \mathbf{u}_\ell d_{k\ell}(\mathbf{A}, \mathbf{R}),$$

where \mathbf{W} is the symmetric $p \times p$ weight matrix containing the individual weights $w_{jj'}$, \mathbf{u}_k represents the k^{th} column of the membership matrix \mathbf{U} and

$$d_{k\ell}^2(\mathbf{A}, \mathbf{R}) = (a_{kk} - a_{\ell\ell})^2 + (p_k - 1)(r_{kk} - r_{k\ell})^2 + (p_\ell - 1)(r_{\ell\ell} - r_{k\ell})^2 + \sum_{\substack{m=1 \\ m \notin \{k, \ell\}}}^K p_m (r_{km} - r_{\ell m})^2.$$

Full details of this derivation are provided in Appendix A.

We are now ready to optimize the objective function $L(\mathbf{A}, \mathbf{R})$, which can be done efficiently—especially as the number of clusters K decreases.

2.3 Cyclic Block Coordinate Descent Algorithm

We propose a cyclic block coordinate descent algorithm to minimize objective function (5) under the constraints from (2), where the blocks are formed by the clusters of variables. To permit cyclic block updates, the objective $L(\mathbf{A}, \mathbf{R})$ needs to be separated into those parts that depend on cluster k , namely a_{kk} , \mathbf{r}_k , and r_{kk} , and those that do not. The $K - 1$ vector \mathbf{r}_k contains the elements of the k^{th} column of \mathbf{R} excluding r_{kk} . We distinguish \mathbf{r}_k and r_{kk} because the diagonal elements of \mathbf{R} interact differently with the objective function compared to other elements related to the k^{th} cluster. Additionally, we partition the objective function into four distinct components, as given by

$$L(a_{kk}, \mathbf{r}_k, r_{kk}) = L_{\text{det}}(a_{kk}, \mathbf{r}_k, r_{kk}) + L_{\text{cov}}(a_{kk}, \mathbf{r}_k, r_{kk}) + L_{\text{cpath}}(a_{kk}, \mathbf{r}_k, r_{kk}) + C, \quad (6)$$

where L_{\det} (L_{cov}) represents the log-determinant (trace) part of the objective function that depends on cluster k , L_{cpath} is the clusterpath penalty that depends on cluster k , and finally C is a constant collecting parts that are independent of cluster k . Details of these expressions are given in Appendix B.

The proposed algorithm now involves two key steps. For each cluster k , it first assesses whether there is an eligible fusion candidate. In the instances where no suitable candidate is identified, the algorithm proceeds to the second step, wherein the parameters associated with cluster k are updated using Newton’s method. The reason we choose a cyclic block coordinate descent algorithm lies with the use of Newton’s method since the computation of a Newton descent direction for all parameters in \mathbf{A} and \mathbf{R} simultaneously would result in a computationally intractable algorithm even for moderately sized data sets.

In Section 2.3.1, we provide details on the two key steps of the optimization algorithm. We further discuss two important components related to the clusterpath penalty, namely the weight matrix (Section 2.3.2) and the tuning parameter (Section 2.3.3). Finally, in Section 2.3.4, we discuss a refitting step to reduce bias in the CGGM estimate.

2.3.1 Outline of the Cyclic Block Coordinate Descent Algorithm

We outline the two-step algorithm minimizing the objective function in (6) iteratively for cluster $1 \leq k \leq K$ for a fixed value for λ .

Cluster fusions. The first step is to verify whether cluster k is close enough to another cluster to warrant their fusion. Cluster k is fused with cluster ℓ if $d_{k\ell}(\mathbf{A}, \mathbf{R})$ is smaller than some user-defined threshold ε_f representing the minimum required similarity for fusion. To account for the scale of the data, we take $\varepsilon_f = \tau \text{median}_{j,j'}(d_{jj'}(\Theta))$, where we typically set $\tau = 10^{-3}$ in our experiments. In case of multiple candidates for which this applies, cluster ℓ is chosen as $\ell = \text{argmin}_{\ell'} d_{k\ell'}(\mathbf{A}, \mathbf{R})$. If a fusion is performed, the algorithm does not proceed to the next step as cluster k has ceased to exist, instead it advances to the next cluster. If no eligible fusion candidate is found in the first step, we proceed to the second step.

Descent direction. The second step is to compute a descent direction. We opt for a Newton descent direction as it offers efficient convergence properties. Let $\nabla L(a_{kk}, \mathbf{r}_k, r_{kk})$ denote the gradient and $\nabla^2 L(a_{kk}, \mathbf{r}_k, r_{kk})$ the Hessian of $L(a_{kk}, \mathbf{r}_k, r_{kk})$, see Appendix B for their derivations. The descent direction is then computed as $\delta_k = -\nabla^2 L(a_{kk}, \mathbf{r}_k, r_{kk})^{-1} \nabla L(a_{kk}, \mathbf{r}_k, r_{kk})$.

Finally, we determine the optimal step size s^* given the descent direction using a line search. The reason for augmenting the Newton descent direction with a line search is twofold. First, the minimization of $L(a_{kk}, \mathbf{r}_k, r_{kk})$ is constrained by the restriction that Θ should be positive definite. Hence, a step size should be chosen that ensures the update to adhere this restriction. Assuming that Θ is positive definite for the current values of $[a_{kk}, \mathbf{r}_k, r_{kk}]$ and the number of clusters is larger than one, positive definiteness of Θ is

preserved by a step size s that satisfies

$$\begin{aligned} (a_{kk} + s\delta_{a_{kk}}) + (p_k - 1)(r_{kk} + s\delta_{r_{kk}}) - p_k(\mathbf{r}_k + s\boldsymbol{\delta}_{\mathbf{r}_k})^\top \mathbf{V}(\mathbf{r}_k + s\boldsymbol{\delta}_{\mathbf{r}_k}) &> 0 \\ a_{kk} + s\delta_{a_{kk}} - r_{kk} - s\delta_{r_{kk}} &> 0, \end{aligned} \quad (7)$$

where $\delta_{a_{kk}}$, $\boldsymbol{\delta}_{\mathbf{r}_k}$, and $\delta_{r_{kk}}$ represent the descent directions for a_{kk} , \mathbf{r}_k , and r_{kk} . In case there is a single cluster left, the first inequality reduces to

$$(a_{kk} + s\delta_{a_{kk}}) + (p_k - 1)(r_{kk} + s\delta_{r_{kk}}) > 0. \quad (8)$$

A second reason to opt for a line search is the fact that the Hessian may not be well-behaved due to the presence of the ℓ_2 -norm in the clusterpath penalty. If, for the current values of \mathbf{A} and \mathbf{R} , at least one of the distances $d_{k\ell}(\mathbf{A}, \mathbf{R})$ is close to zero, $L(a_{kk}, \mathbf{r}_k, r_{kk})$ is not locally smooth. As a result, the Hessian is not well-behaved and the favorable convergence properties of Newton's method do not hold. A line search for the optimal step size guarantees that the update $s^*\boldsymbol{\delta}_k$ does not increase the objective function.

The pseudo-code for the algorithm is presented in Algorithm 1. To initialize \mathbf{A} and \mathbf{R} , one can use the inverse of the sample covariance matrix if it is available; then $\mathbf{A}^{(1)} = \text{diag}(\mathbf{S}^{-1})$ and $\mathbf{R}^{(1)} = \mathbf{S}^{-1}$. In other cases, one can start from a regularized estimator such as the graphical lasso (Yuan & Lin, 2007; Banerjee et al., 2008; Rothman et al., 2008; Friedman et al., 2008).

2.3.2 Weight Matrix

An important element of the clusterpath estimator is the weight matrix \mathbf{W} that contains information about the preferences of clustering variables j and j' through the weight $w_{jj'}$. A large value for $w_{jj'}$ incentivizes clustering of the corresponding variables, but it does not guarantee this. In the convex clustering literature, it is standard practice to set the weights based on the distances between the original data points (see, e.g., Chi et al., 2017; Hocking et al., 2011; Sun et al., 2021). Furthermore, clustering performance increases when using k -nearest neighbors to assign zero weights to pairs of variables that are beyond each other's k nearest neighbors (Chi & Lange, 2015). Following these standard practices, we take

$$w_{jj'} = w_{j'j} = \begin{cases} \exp(-\phi d_{jj'}^2(\mathbf{S}^{-1})) & \text{if } (j, j') \in \mathcal{E} \\ 0 & \text{otherwise,} \end{cases}$$

where ϕ is a tuning parameter and \mathcal{E} is the set of variable-pairs (j, j') that should be assigned a nonzero weight.

A potential issue with relying solely on k -nearest neighbors for the construction of \mathcal{E} is the occurrence of disconnected subgroups. To alleviate this issue, we add variable-pairs to \mathcal{E} using the procedure described in Kruskal (1956) until all disconnected subgroups are eliminated. This approach effectively integrates the

Algorithm 1 Pseudo-code for the algorithm that minimizes the CGGM objective function for fixed λ .

Input Initial estimates for $\mathbf{A}^{(1)}$ and $\mathbf{R}^{(1)}$, sample covariance matrix \mathbf{S} , weight matrix \mathbf{W} , tuning parameter λ , fusion threshold ε_f , convergence threshold ε_c , maximum number of iterations t_{\max}

Output $\hat{\mathbf{A}}$ and $\hat{\mathbf{R}}$ that minimize $L(\mathbf{A}, \mathbf{R})$ with $\hat{\mathbf{U}}$ that describes cluster membership

```

1:  $\mathbf{U}^{(1)} \leftarrow \mathbf{I}$ 
2:  $L^{(1)} \leftarrow L(\mathbf{A}^{(1)}, \mathbf{R}^{(1)})$ 
3:  $L^{(0)} \leftarrow (1 + 2\varepsilon_c)L^{(1)}$ 
4:  $t \leftarrow 1$ 
5: while  $L^{(t-1)}/L^{(t)} - 1 > \varepsilon_c$  and  $t \leq t_{\max}$  do
6:    $t \leftarrow t + 1$ 
7:    $\mathbf{A}^{(t)} \leftarrow \mathbf{A}^{(t-1)}$ 
8:    $\mathbf{R}^{(t)} \leftarrow \mathbf{R}^{(t-1)}$ 
9:    $\mathbf{U}^{(t)} \leftarrow \mathbf{U}^{(t-1)}$ 
10:  for  $k = 1, \dots, K$  do
11:     $\ell \leftarrow \operatorname{argmin}_{\ell'} d_{k\ell'}(\mathbf{A}^{(t)}, \mathbf{R}^{(t)})$ 
12:    if  $d_{k\ell}(\mathbf{A}^{(t)}, \mathbf{R}^{(t)}) \leq \varepsilon_f$  then
13:      Fuse clusters  $k$  and  $\ell$  by modifying  $\mathbf{A}^{(t)}, \mathbf{R}^{(t)}, \mathbf{U}^{(t)}$ 
14:    else
15:       $\delta_k \leftarrow -\nabla^2 L(a_{kk}^{(t)}, \mathbf{r}_k^{(t)}, r_{kk}^{(t)})^{-1} \nabla L(a_{kk}^{(t)}, \mathbf{r}_k^{(t)}, r_{kk}^{(t)})$ 
16:      Compute maximum step size  $s_{\max}$  using equations (7) and (8)
17:      Select optimal step size  $s^* \in [0, s_{\max})$ 
18:       $[a_{kk}^{(t)}, \mathbf{r}_k^{(t)}, r_{kk}^{(t)}] \leftarrow [a_{kk}^{(t)}, \mathbf{r}_k^{(t)}, r_{kk}^{(t)}] + s^* \delta_k$ 
19:   $\hat{\mathbf{A}} \leftarrow \mathbf{A}^{(t)}$ 
20:   $\hat{\mathbf{R}} \leftarrow \mathbf{R}^{(t)}$ 
21:   $\hat{\mathbf{U}} \leftarrow \mathbf{U}^{(t)}$ 

```

k -nearest neighbors structure with a minimum spanning tree to obtain a weight matrix corresponding to a connected graph (Touw et al., 2022).

2.3.3 Tuning Parameters

The tuning parameter λ forms another key ingredient of the clusterpath estimator as it controls the degree of clustering. First, note that in the current form of objective function (3), the tuning parameter λ is sensitive to the number of variables p . To reduce this sensitivity, the different terms of the objective function may be scaled. We suggest to scale the terms pertaining to the log likelihood by p^{-1} and the penalty by $\kappa = ((p-1)^{1/2} \sum_{j < j'} w_{jj'})^{-1}$ to reduce this dependence on p . These scaling factors can then easily be absorbed into a rescaled tuning parameter $\gamma = p\kappa\lambda$, which then replaces λ in the objective function.

To set a sequence of tuning parameters, we implement an automated procedure. First, λ is initialized at 0.5 and undergoes iterative increments of 50% until the minimum number of clusters, as determined by the weight matrix, is attained. This yields an increasing series of values $\{\lambda_q : 1 \leq q \leq Q\}$ alongside their corresponding solutions $\{\hat{\Theta}_q : 1 \leq q \leq Q\}$. To ensure smoothness in the trajectory, additional values of λ are inserted whenever the difference between consecutive solutions, as measured by $\|\hat{\Theta}_{q-1} - \hat{\Theta}_q\|/\|\hat{\Theta}_{q-1}\|$, exceeds 0.01. Consequently, a continuum of solutions for Θ is obtained, transitioning smoothly from minimal to maximal regularization, with a hierarchical clustering structure. Throughout this iterative process, the algorithm leverages existing solutions for the precision matrix as warm starts to speed up finding solutions for new values of λ .

Apart from the tuning parameter λ that controls the degree of clustering, one also needs to select the tuning parameters k and ϕ that are used to compute the weight matrix. Typical values of interest for k range from 1 to $p^{1/2}$. The choice for ϕ depends heavily on the scale of the data. The smallest value of ϕ that is of interest ensures that most nonzero weights lie between 0.9 and 1.0, whereas the largest value results in a more uniform distribution of the nonzero weights.

To select the tuning parameters λ , k , and ϕ we adopt a cross-validation procedure. We form a grid of tuning parameters (λ, k, ϕ) and find the combination of the tuning parameters that minimizes the cross-validated likelihood-based score given by

$$\frac{1}{G} \sum_{g=1}^G -\log |\hat{\Theta}_{-\mathcal{F}_g}| + \text{tr} \mathbf{S}_{\mathcal{F}_g} \hat{\Theta}_{-\mathcal{F}_g}, \quad (9)$$

where $\hat{\Theta}_{-\mathcal{F}_g}$ represents the precision matrix estimated on the sample excluding the observations in the g^{th} fold ($1 \leq g \leq G$, one can take for instance $G = 5$), and $\mathbf{S}_{\mathcal{F}_g}$ denotes the sample covariance matrix computed solely on the samples within the g^{th} fold. The density of the grid for k and ϕ depends on p ; low-dimensional data allows for shorter computation times and denser grids. In this paper, we use grids of five to eight evenly spaced values for both tuning parameters.

2.3.4 Refitted CGGM

While minimization of the objective function in (5) yields a clustered $\widehat{\Theta}$, the CGGM estimate may be biased due to the shrinkage of the distances between different clusters. Following Wilms & Bien (2022), we therefore also consider a refitted version of CGGM. First, CGGM is used to obtain a clustering in $\widehat{\Theta}$, as defined by the cluster membership estimate $\widehat{\mathbf{U}}$. We then re-estimate the precision matrix Θ constrained by the obtained clustering by maximizing the likelihood subject to the clustering constraint. This is equivalent to minimizing the objective in (5) with initial clustered estimates for \mathbf{A} and \mathbf{R} and $\lambda = 0$. By re-estimating the precision matrix, we aim to capitalize on the clustering capabilities of CGGM while refining parameter estimates for improved accuracy.

2.4 Connections to Related Work

Clustering in the context of GGMs arises either at the level of the observations¹ or at the level of the variables (i.e., the nodes). Here, we focus on GGMs with clustered nodes. Contributions to this strand of the literature can be divided into three main streams.

A first stream assumes one can *a priori* cluster the variables into *known* groups which share similar dependencies (e.g., Duchi et al., 2008; Schmidt et al., 2009; Grechkin et al., 2015; Millington & Niranjana, 2019). Domain-knowledge may, however, not always be available to impose a grouping, thereby still calling for unsupervised clustering procedures. A second stream of papers therefore uses *two-step sequential procedures* that first learn how to cluster the variables and then turn to the estimation of the GGM (e.g., Ambroise et al., 2009; Marlin & Murphy, 2009; Tan et al., 2015; Eisenach et al., 2020; Brownlees et al., 2022). A two-step procedure that decouples the clustering step from the GGM estimation may, however, lead to suboptimal results, thereby giving rise to a third stream that considers both tasks jointly.

In this third stream, Nie et al. (2016), Kumar et al. (2020), Cardoso et al. (2020), and Gheche & Frossard (2020), amongst others, study *k*-connected component graphs permitting variable clustering in *k* groups due to the spectral properties of the Laplacian matrix. Besides, penalized likelihood procedures form a popular alternative to encourage various forms of node-clustering (e.g., Hosseini & Lee, 2016; Tarzanagh & Michailidis, 2018). To this end, our proposal is most closely related to Yao & Allen (2019), Pircalabelu & Claeskens (2020), and Wilms & Bien (2022).

The first to explore the use of a clusterpath penalty in precision matrix estimation are Yao & Allen (2019). However, a key distinction with our proposal lies in the distance metric used in the penalty: their approach does not account for the diagonal elements of Θ whereas ours does. This is an important distinction in the

¹A separate literature stream thus considers GGMs where the *observations* come from different subpopulations (i.e. clusters) that are either *a priori* known (e.g., Danaher et al., 2014; Mohan et al., 2014) or learned from the data by unifying clustering with GGM estimation into one optimization framework (e.g., Gao et al., 2016; Hao et al., 2018).

context of GGMs since variables clustered by CGGM share identical values on the diagonal of the precision matrix. As a consequence, unlike for the proposal of Yao & Allen (2019), the clustering in $\hat{\Theta}$ is retained in its inverse (see, e.g., Gower & Groenen, 1991; Archakov & Hansen, 2022). Pircalabelu & Claeskens (2020) use a penalized likelihood procedure with a group penalty to identify communities of nodes, their procedure—unlike ours—does not result in a precision matrix with block structure. Wilms & Bien (2022), finally, use a penalized likelihood procedure with a tree-based penalty to cluster nodes, hence their choice of penalty differs from ours as it requires side-information on the similarity of nodes to guide their clustering. We include the proposals of Pircalabelu & Claeskens (2020) and Wilms & Bien (2022) as benchmarks in our simulation study since their software implementations are publicly available.

3 Simulations

To investigate the behavior of the proposed method CGGM, we perform an extensive simulation study. We discuss the data generating processes in Section 3.1, the benchmark methods and evaluation criteria in Section 3.2, and the results in Section 3.3.

3.1 Simulation Designs

For most of the simulations, we follow the designs of Wilms & Bien (2022) together with some additional variations. In all settings, we sample data from a multivariate normal distribution with mean zero and covariance matrix $\Sigma = \Theta^{-1}$, and we repeat the process 100 times.

Baseline simulation designs. We simulate $n = 120$ observations on $p = 15$ variables using four different structures for the precision matrix Θ (see Figure 2, top row):

- *Random:* The clusters are of equal size with $p_1 = p_2 = p_3 = 5$; one pair of clusters is selected at random to be connected via an edge.
- *Chain:* The clusters are of equal size with $p_1 = p_2 = p_3 = 5$; adjacent clusters are connected via an edge.
- *Unbalanced:* Same as the chain design, but the clusters are of unequal size with $p_1 = 3$, $p_2 = 5$, and $p_3 = 7$.
- *Unstructured:* Each variable forms its own cluster; edges between variables are drawn with probability $\pi = 0.1$.

The first three designs thus employ a block structure with $K = 3$ clusters, while the fourth does not exhibit any variable aggregation structure. In all four designs, the diagonal elements of Θ are set to 1, the elements within a cluster of variables to 0.5, and the non-zero elements between clusters to 0.25.

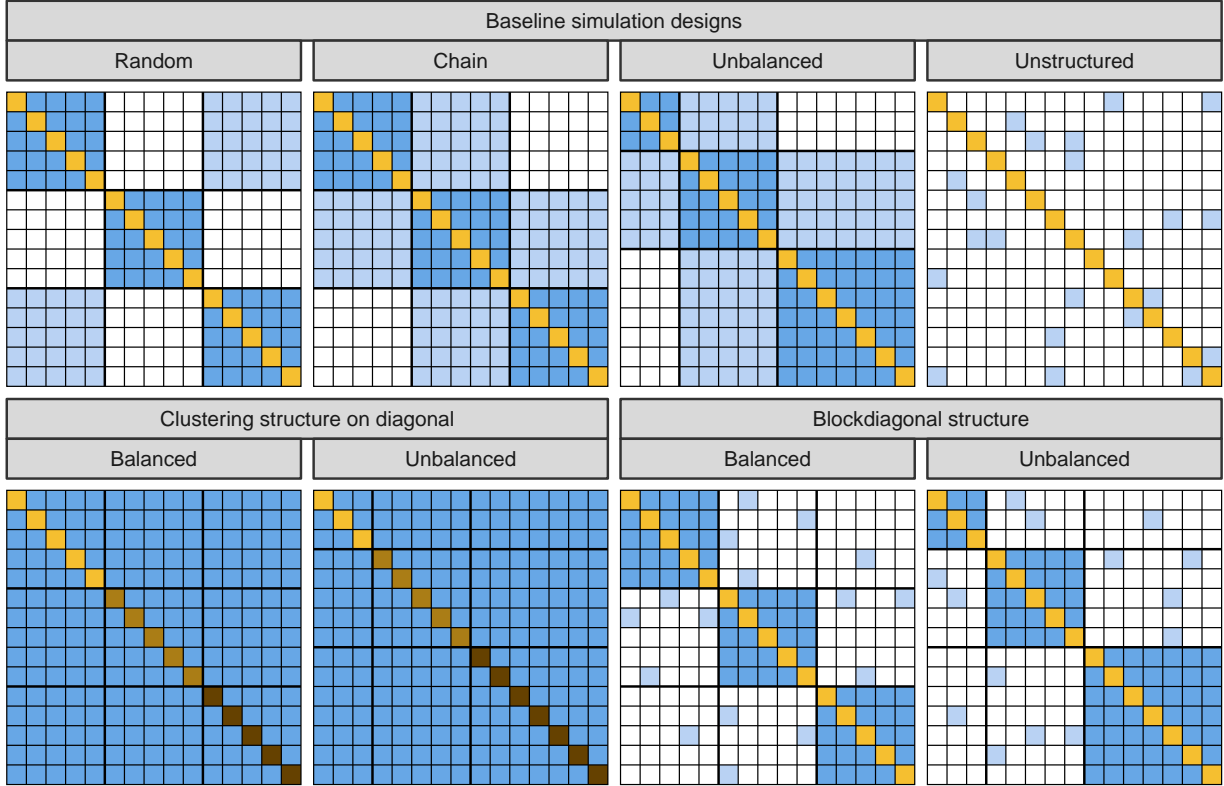


Figure 2: Structure in the precision matrix Θ in the four baseline simulation designs taken from Wilms & Bien (2022) (top), as well as in the designs with clustering structure on the diagonal and with blockdiagonal structure, respectively, using balanced and unbalanced clusters sizes (bottom). The color shade indicates the magnitude of the elements. Diagonal elements are on a separate color scale than the off-diagonal ones to highlight their differing roles in CGGM in comparison to the benchmark methods.

Increasing the number of variables. We focus on the chain design as in Wilms & Bien (2022) and vary the number of variables $p \in \{15, 30, 60\}$. We set the corresponding number of observations $n \in \{120, 240, 480\}$ such that the ratio n/p is constant. The number of clusters is kept fixed at $K = 3$.

Increasing the number of clusters. We again focus on the chain design and vary the number of clusters $K \in \{3, 5, 6, 10\}$ while keeping the number of observations and variables fixed at $n = 240$ and $p = 30$, respectively, as in Wilms & Bien (2022).

Approximate block structure. We take the four baseline designs and modify the structure in Θ by uniformly drawing elements within a cluster of variables from the interval $[0.4, 0.6]$ and non-zero elements between clusters from the interval $[0.2, 0.3]$. The assumptions of CGGM are not (fully) met in the resulting designs, as the clusters do not correspond to blocks of equal values in Θ but blocks of approximately similar values.

Clustering structure on diagonal. Using the same dimensions and number of clusters as in the baseline designs, all off-diagonal elements in Θ are set to 0.5. The diagonal elements are set to 1 for the variables in the first cluster, to 2 for the variables in the second cluster, and to 3 for the variables in the third cluster. We investigate both a *balanced* design with $p_1 = p_2 = p_3 = 5$, and an *unbalanced* design with $p_1 = 3$, $p_2 = 5$, and $p_3 = 7$ (see left two panels in the bottom row of Figure 2).

Blockdiagonal structure. In these designs, the precision matrix Θ does not exhibit a variable clustering structure, but a blockdiagonal structure inspired by the simulation design of Pircalabelu & Claeskens (2020). We use the same dimensions as in the baseline design and $K = 3$ blocks on the diagonal. Outside of the diagonal blocks, edges between variables are drawn with probability $\pi = 0.1$. The diagonal values of Θ are set to 1, the off-diagonal elements in the diagonal blocks are set to 0.5, and non-zero elements outside the diagonal blocks are set to 0.25. If such a randomly drawn precision matrix is not positive semi-definite, we repeat this process until a positive semi-definite precision matrix is obtained. We consider both a *balanced* design with $p_1 = p_2 = p_3 = 5$, and an *unbalanced* design with $p_1 = 3$, $p_2 = 5$, and $p_3 = 7$ (see the right two panels in the bottom row of Figure 2).

3.2 Methods and Evaluation Criteria

We apply CGGM with and without the parameter re-estimation step described in Section 2.3.4, which we refer to as *CGGM-raw* and *CGGM-refit*. We thereby set the convergence tolerance $\varepsilon_c = 10^{-7}$ and the maximum number of iterations to $t_{\max} = 5000$. For comparison, we include the tree-aggregated graphical lasso (*TAGL*) of Wilms & Bien (2022), the community-based group graphical lasso (*ComGGL*) of Pircalabelu & Claeskens (2020), and the inverse of the sample covariance matrix (\mathbf{S}^{-1}). TAGL performs node aggregation based on side-information in the form of a tree-based variable hierarchy, which needs to be specified a priori. We generate an *ideal* and a *realistic* tree hierarchy as described in Wilms & Bien (2022) (see Figure 5 in their paper for an illustration). As both trees contain the true variable clustering, we also generate a *misspecified* tree in the same manner as the realistic tree, except that with probability 0.1, each variable is incorrectly assigned to the subsequent cluster (or the first cluster if the variable in fact belongs to the last cluster). ComGGL does not perform node aggregation but community detection in the form of a blockdiagonal structure. As opposed to CGGM, both TAGL and ComGGL also apply lasso-regularization for edge sparsity.

Concerning tuning parameter selection, we apply 3-fold cross-validation. For the weight matrix in CGGM, we use candidate values $\phi \in \{1, 1.5, 2, 2.5, 3\}$ and numbers of neighbors $k \in \{1, 2, 3, 4, 5\}$. For each combination of ϕ and k , we select candidate values for the regularization parameter λ as described in Section 2.3.3. For TAGL, we first perform a binary search for the smallest value of the aggregation parameter that aggregates all variables into one cluster (for each of the tree hierarchies) while keeping the sparsity parameter

at 0, and we determine the smallest value of the sparsity parameter that removes all edges while keeping the aggregation parameter at 0 (corresponding to the graphical lasso of Friedman et al., 2008). The candidate values for the aggregation and sparsity parameters are then obtained as fractions of those aforementioned values, where the fractions vary from 0 to 1 in 10 steps, with each step being twice as large as the previous step. For ComGGL, we similarly set the candidate values of the grouping and sparsity parameters as fractions of certain maximum values. While we fix the maximum value of the grouping parameter at 1, we again set the maximum value of the sparsity parameter as the smallest value that removes all edges in the graphical lasso. As in Pircalabelu & Claeskens (2020), we set the balancing parameter to 1.

We evaluate the methods in terms of their estimation accuracy and aggregation performance. Regarding estimation accuracy, we compute the Frobenius norm $\|\Theta - \hat{\Theta}\|_F$. For aggregation performance, we report the estimated number of clusters \hat{K} as well as the adjusted Rand index (ARI) (Hubert & Arabie, 1985) of the obtained clustering of variables. Note that \hat{K} directly follows from the obtained clustering for the optimal values of the tuning parameters from cross-validation.

3.3 Results

In Figures 3–5, we report the evaluation criteria for different simulation designs. As CGGM and TAGL outperform ComGGL and the inverse of the sample covariance matrix (\mathbf{S}^{-1}) in almost all cases, we focus on the former two methods in the following discussion of the results.

Baseline simulation designs. In terms of estimation accuracy and aggregation, CGGM-raw and CGGM-refit perform similar to TAGL-ideal, outperform TAGL-realistic in some designs, and outperform and TAGL-misspecified in all designs (see Figure 3). The refitting step of CGGM is advantageous in the three block designs but disadvantageous in the unstructured design. For the latter, the refitting step often aggregates all variables into one cluster, likely due to the high degree of sparsity in the unstructured design. This pooling of estimates for the large number of zero elements reduces noise, potentially improving the out-of-sample cross-validation score in equation (9), despite introducing some bias in the relatively small number of nonzero elements. Conversely, CGGM-raw allows for shrinkage between elements without aggregation, thus improving estimation performance for designs in which many off-diagonal elements share the same value without belonging to the same cluster. While TAGL-misspecified often selects the correct number of clusters, the ARI reveals that it struggles to accurately classify the variables within those clusters due to the misspecified tree. This pattern persists across most of the simulation designs.

Increasing the number of variables or clusters. Given that CGGM-refit clearly outperforms CGGM-raw in the baseline chain design, we omit the results for the latter in the variations with increasing number of variables or clusters. First, the results remain stable when increasing the number of variables and are similar to those in the baseline setting (see Figure 10 in Appendix C), likely due to maintaining a fixed

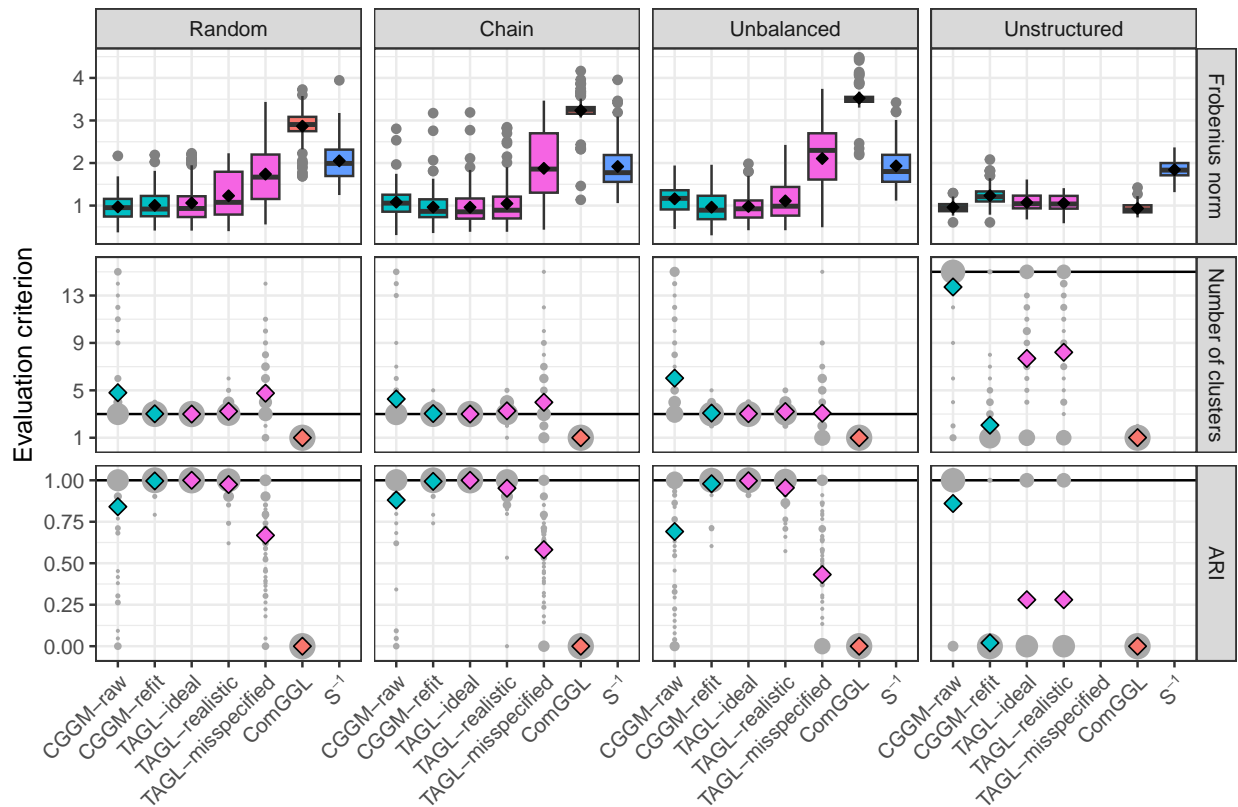


Figure 3: Results for the baseline simulation designs (in separate columns). The top row contains boxplots of the Frobenius norm together with black diamonds representing the average. In the middle and bottom rows, diamonds display the average of the estimated number of clusters and the average ARI, respectively. In addition, the size of the grey dots represent the frequency of different values across the replications. Reference lines are drawn for the true number of clusters and the maximum possible ARI value. Aggregation performance is omitted for \mathbf{S}^{-1} as it does not perform any aggregation. In the unstructured design, a misspecified tree for TAGL does not exist since any tree hierarchy contains the true clustering (each variable being its own cluster).

ratio of n to p . CGGM-refit performs comparably to TAGL-ideal and TAGL-realistic, and clearly surpasses TAGL-misspecified. Second, as the number of clusters increases, the aggregation performance of CGGM-refit remains stable, although the estimation error in terms of the Frobenius norm increases (see Figure 4). In the chain design, the sparsity of the precision matrix increases in the number of clusters. Hence, a method that enforces sparsity—such as TAGL—is expected to perform well, particularly when up to 56% of the elements are zero (as in the design with $K = 10$). While the median estimation error of CGGM-refit increases in comparison to TAGL-ideal and TAGL-realistic, it remains considerably lower than that of TAGL-misspecified. To investigate estimation performance further, we also considered the negative log-likelihood

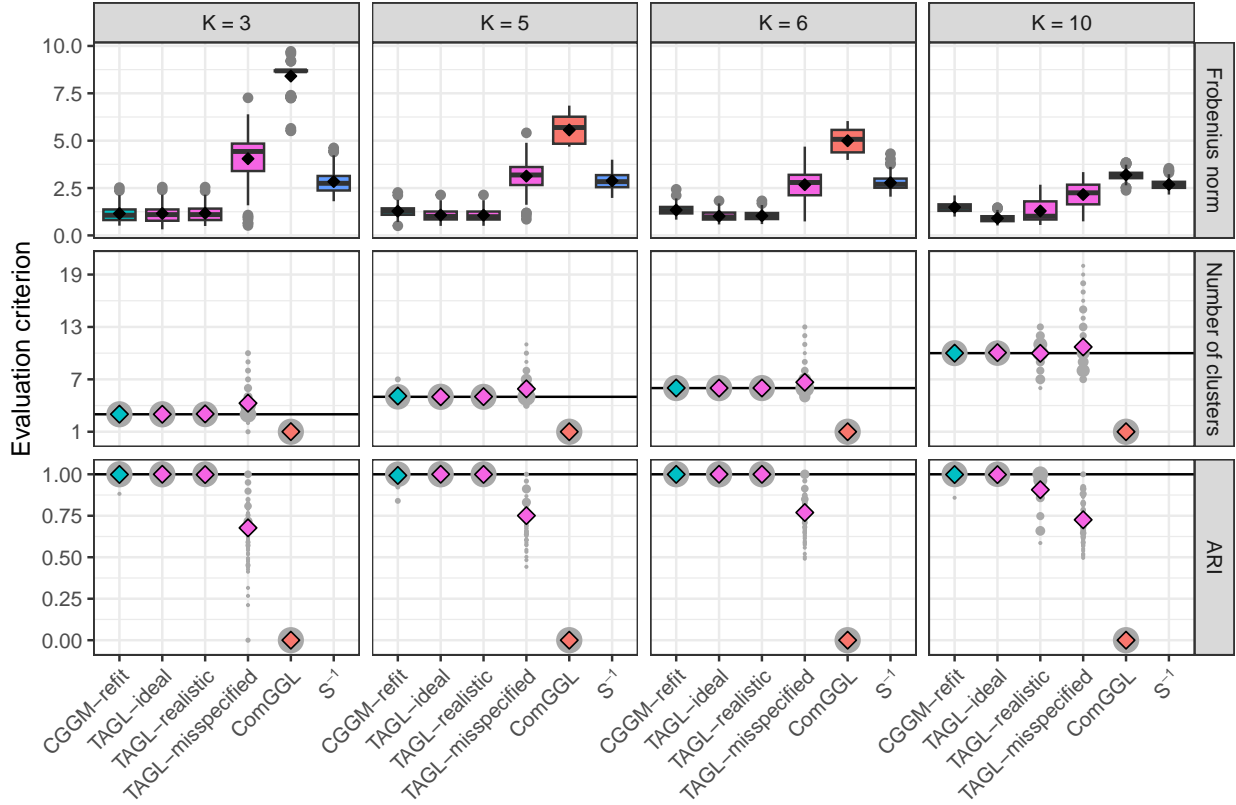


Figure 4: Results for the chain simulation design with an increasing number of clusters (in separate columns). See Figure 3 for explanatory notes.

of the estimated precision matrix, which remains similar for CGGM-refit and TAGL-ideal as the number of clusters increases (results not shown). Finally, CGGM-refit in some settings exhibits lower variability in the estimation error compared to TAGL-realistic.

Approximate block structure. The results for estimation accuracy are highly similar to those of the baseline simulation designs (see Figure 11 in Appendix C). In terms of aggregation performance, CGGM-raw struggles to find the block structure when it is no longer exact, but the refitting step overcomes this issue. TAGL-realistic also performs worse in terms of aggregation, though the effect is less pronounced than with CGGM-raw. Overall, aggregation performance of CGGM-refit and TAGL-ideal remains very similar to the baseline designs. It is important to note that, technically, the identified block structure is incorrect at the population level. However, the noise reduction in finite samples is still beneficial.

Clustering structure on diagonal. CGGM-refit clearly outperforms the alternative methods in terms of aggregation performance (see left two columns in Figure 5). All variants of TAGL tend to aggregate all variables into one cluster, as they exclude the elements on the diagonal from the aggregation penalty. As a result, the variability in the estimation error of TAGL is considerably larger compared to CGGM. Despite the

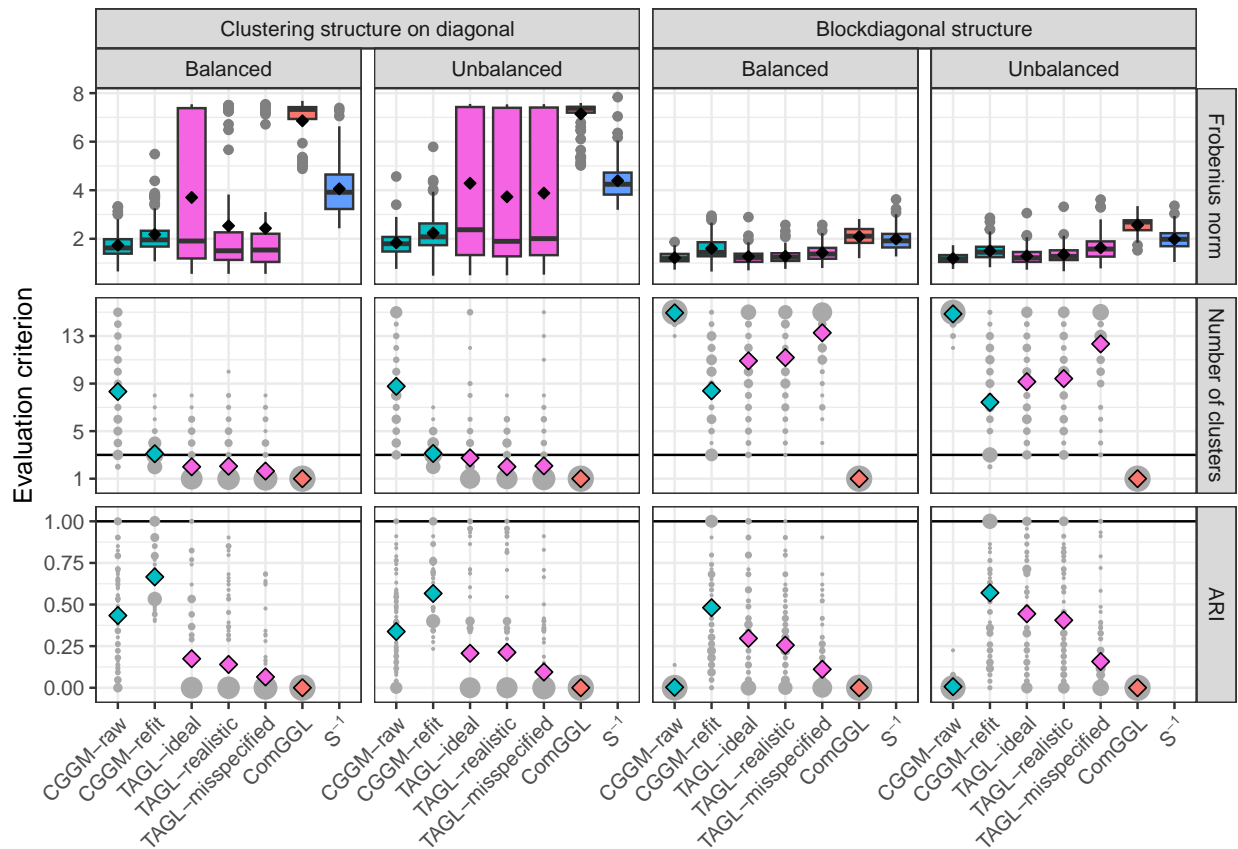


Figure 5: Results for the simulation designs with the clustering structure on the diagonal (left two columns) and with a blockdiagonal structure (right two columns). See Figure 3 for explanatory notes.

better aggregation performance, the estimation error is slightly higher for CGGM-refit than for CGGM-raw. A likely explanation of this phenomenon is that CGGM-refit no longer applies shrinkage to the difference between elements from different clusters. In this design, this behavior does not align with the structure of the underlying precision matrix, in which all off-diagonal elements share the same value. Consequently, by shrinking the off-diagonal elements from different clusters towards each other, CGGM-raw achieves superior estimation accuracy even without finding the true cluster structure.

Blockdiagonal structure. In evaluating aggregation performance, CGGM-refit demonstrates a sizeable advantage over alternative methods (see right two columns in Figure 5). However, it exhibits a slightly higher estimation error compared to CGGM-raw, TAGL-ideal, and TAGL-realistic. As in the designs with an approximate block structure, it is worth noting that the identified block structure is technically incorrect at the population level. Nonetheless, identifying groups remains beneficial, considering the limited number of nonzero elements outside the diagonal blocks. Furthermore, the performance of CGGM-raw is noteworthy, as it surpasses all alternatives in terms of estimation accuracy with minimal aggregation.

Conclusions from the simulations. CGGM-refit exhibits excellent performance similar to TAGL-ideal while not requiring auxiliary information. Additionally, the simulations reveal that a misspecification of the tree that encodes the aggregation is detrimental to the performance of TAGL, positioning CGGM as a particularly strong alternative when accurate information on the aggregation structure is unavailable. Notably, CGGM consistently keeps up with—and even surpasses—alternatives in simulation designs characterized by a clear sparsity structure, despite the absence of a penalty term specifically aimed at identifying such patterns. In general, the refitting step is beneficial, but may lead to overaggregation in unstructured settings. Correspondingly, in some scenarios, we find that there is a trade-off between CGGM-raw and CGGM-refit in terms of estimation accuracy and aggregation performance.

4 Estimation of a Clustered Covariance Matrix

While this paper so far has been focused on estimating a clustered precision matrix in order to simplify the partial dependency structure among the variables, it can also be of interest to obtain a clustered covariance matrix. For instance, a block structure in the covariance matrix implies that the variables of a given block have equal loadings in latent factor models. In this context, a clustered covariance matrix may reduce uncertainty in estimating the latent factors.

Contrary to other approaches for finding block structures in the precision matrix, such as those of Yao & Allen (2019), Pircalabelu & Claeskens (2020), and Wilms & Bien (2022), CGGM retains the found block structure when taking the inverse of the obtained estimate (see Section 2.1). If model (1) holds for the precision matrix Θ , it may therefore be reasonable to obtain a clustered estimate of the covariance matrix Σ by taking $\hat{\Sigma} = \hat{\Theta}^{-1}$, where $\hat{\Theta}$ denotes the estimate of the precision matrix from CGGM. However, adherence to an exact block structure as in model (1) may be a rather strong assumption in practice. If this model only holds approximately with somewhat similar values within the blocks of Θ , we have seen in the simulations that estimating a clustered precision matrix with CGGM is nevertheless beneficial. But if an approximate block structure is present in the covariance matrix Σ , the structure in Θ is much more noisy with larger variability between the elements in the corresponding blocks, as illustrated in Figure 6. In such settings, first estimating a clustered precision matrix with CGGM and then taking the inverse may not succeed in finding the correct structure.

To estimate a clustered covariance matrix, one could attempt to adapt the clusterpath algorithm to be based on the objective function

$$-\log |\Sigma^{-1}| + \text{tr} \Sigma \Sigma^{-1} + \lambda \mathcal{P}(\Sigma).$$

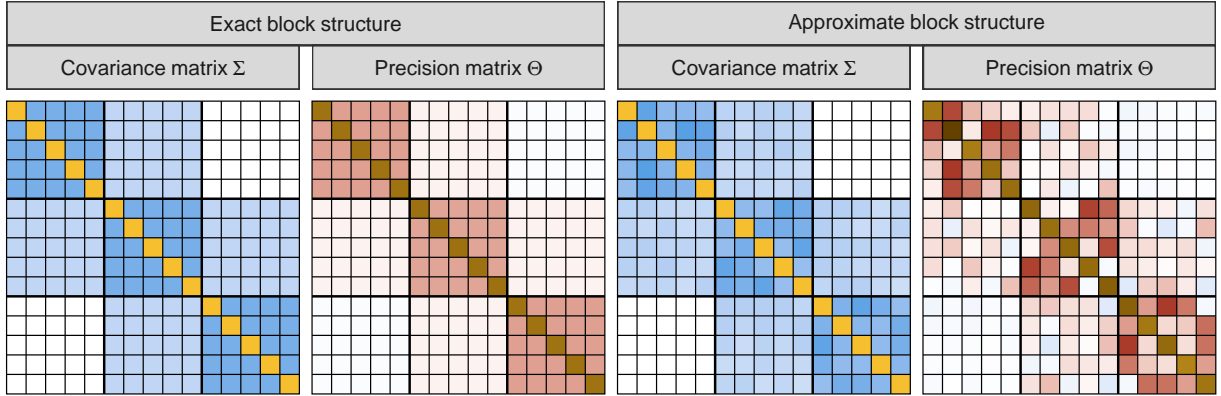


Figure 6: Illustration of how an exact block structure is retained between the covariance matrix Σ and the precision matrix Θ (left), whereas an approximate block structure in Σ corresponds to a much more noisy structure in Θ (right).

An algorithm optimizing this objective function must deal with an additional layer of complexity, as evaluation of Σ is required in the penalty part and evaluation of Σ^{-1} in the likelihood part of the objective function.

As an alternative, consider a random vector \mathbf{X} that follows a normal distribution with covariance matrix Σ . Then there exists an affine transformation matrix $\mathbf{A} = \mathbf{A}(\Sigma)$ so that $\mathbf{Y} = \mathbf{A}^\top \mathbf{X}$ follows a normal distribution with covariance matrix $\Theta = \Sigma^{-1}$. That is, Σ is the precision matrix for the random vector \mathbf{Y} , which implies that we can apply CGGM to minimize the objective function $L(\Sigma)$ from (5) with the following minor modification. As we do not observe realizations of \mathbf{Y} , we cannot compute the sample covariance matrix of those realizations. Instead, we take the inverse of the sample covariance matrix \mathbf{S}^{-1} of the observed realizations of \mathbf{X} as input for the CGGM algorithm.

To study this further, we conduct simulations using the same settings as in the baseline chain design—which employs an exact block structure—and the approximate block structure chain design (see Section 3.1), but with the block structure in the covariance matrix Σ rather than the precision matrix Θ . We apply CGGM for obtaining a clustered precision matrix followed by taking the inverse (denoted by CGGM- $\hat{\Theta}^{-1}$) and the modification for obtaining a clustered covariance matrix (denoted by CGGM- $\hat{\Sigma}$), as well as the sample covariance matrix \mathbf{S} . Both variants of CGGM include the parameter re-estimation step from Section 2.3.4. The results are shown in Figure 7. Clearly, CGGM- $\hat{\Sigma}$ succeeds in finding the relevant structure in most replications whereas CGGM- $\hat{\Theta}^{-1}$ struggles to do so, even for the setting with an exact block structure. While both variants of CGGM improve upon the sample covariance matrix \mathbf{S} in terms of the estimation error, CGGM- $\hat{\Sigma}$ exhibits the lowest error. Although a more thorough evaluation is beyond the scope of this paper, our findings are an indication that applying CGGM- $\hat{\Sigma}$ may be preferable over CGGM- $\hat{\Theta}^{-1}$ when a

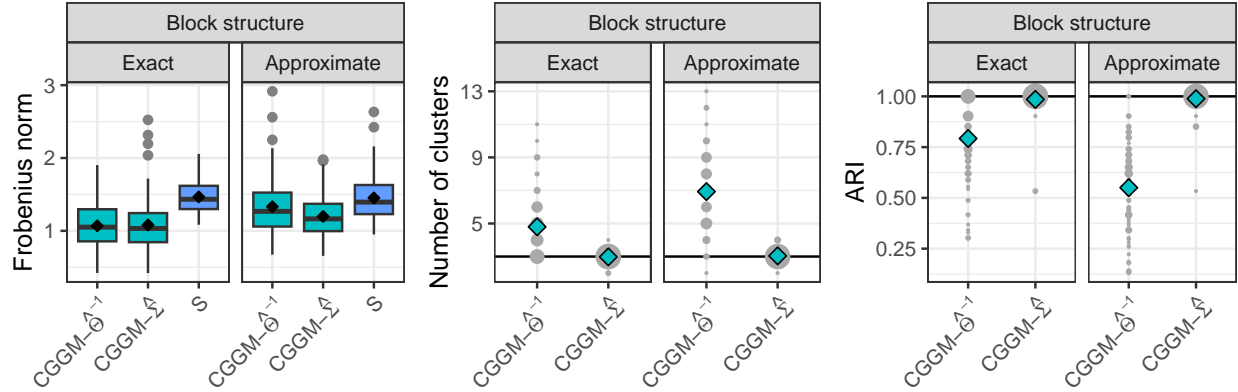


Figure 7: Results for the simulation designs regarding the estimation of a clustered covariance matrix (in separate panels per column). Compare Figure 3 for explanatory notes. Aggregation performance is omitted for the sample covariance matrix \mathbf{S} as it does not perform any aggregation.

clustered covariance matrix is of primary interest. We therefore recommend users to first decide on the object of interest, a block-structured covariance matrix or precision matrix, and then use CGGM accordingly.

5 Applications

We demonstrate the practical usefulness and versatility of CGGM on three applications: a finance application using stock data in Section 5.1, an application with country-level well-being indicators in Section 5.2, and a survey-based behavioral science application in Section 5.3.

5.1 S&P 100 Stocks

Consider a financial data set containing price information of $p = 101$ stocks of the companies that constituted the S&P 100 on September 18th, 2023. Daily stock price information was collected for the period ranging from January 3rd, 2023, until December 29th, 2023 ($n = 250$).² We compute daily realized ranges as given by

$$r_{tj} = \frac{(\log H_{tj} - \log L_{tj})^2}{4 \log 2},$$

where H_{tj} and L_{tj} are the high and low prices for stock j ($j = 1, \dots, p$) during trading day t (Parkinson, 1980) and study the conditional dependency structure of the stocks' realized ranges. As a preprocessing step, we first fit the popular heterogeneous autoregressive (HAR) model of Corsi (2009) to the individual

²The S&P 100 contains 100 companies that may have one or more classes of stocks listed. During the timeframe of our analysis, Alphabet was the sole company with more than one class, distinguished by the symbols GOOG and GOOGL, therefore resulting in $p = 101$ instead of $p = 100$ variables in our analysis.

daily realized range series to capture time dependencies, and then apply CGGM to the standardized residual series to learn the conditional dependency structure among the stocks; our procedure is in line with Wilms & Bien (2022).

We compare the performance of CGGM to that of TAGL. While the former learns how to cluster the variables in an unsupervised data-driven way, the latter requires side-information in the form of a tree that encodes the similarity between the variables stocks to do so. To this end, we use the Global Industry Classification Standard (GICS). The tree then consists of the $p = 101$ stocks (leaves), 11 sectors as middle layer where each stock/company belongs to one industry sector, and one root node that aggregates all sectors. For both methods, we use 5-fold cross-validation to select the tuning parameters (k , ϕ , and λ for CGGM; λ_1 and λ_2 for TAGL) and refit the precision matrix subject to the obtained variable clustering. For the weight matrix in CGGM, we use a grid of $\phi \in \{2, 6, 10, 14, 18, 22\}$ and $k \in \{1, 3, 5, 7, 9, 11, 13, 15\}$ and for TAGL the tuning parameter grid is determined via the same procedure as described in Section 3.2.

The cluster solution returned by both procedures differs considerably. CGGM groups the stocks into $K = 3$ clusters: the first cluster contains BAC (issued by Bank of America Corp.), the second cluster contains GOOG and GOOGL (both issued by Alphabet), and the last one contains the remaining stocks. That is, CGGM puts the Bank of America and the technology company Alphabet in the spotlight as opposed to the rest of the market. TAGL, in contrast, results in $K = 9$ clusters where the industry sectors are assigned to the different clusters on an almost one-to-one basis. In the left panel of Figure 8, we present the distribution of the sectors over the clusters for both CGGM and TAGL. The unbalanced cluster solution of the former versus the more balanced one of the latter directly stands out. The role of the stocks BAC, GOOG, and GOOGL in our analysis is in line with the central, market-wide role of banks (e.g., Martins, 2023) and technology companies (e.g., Cardoso et al., 2020) since their influence on prices affects stocks across the whole market.

Given the considerable difference in clusters returned by both methods, a natural question is how both perform in capturing the conditional dependency structure. To this end, we conduct an out-of-sample exercise to compare their performance. An additional outer loop for 10-fold cross-validation is used to compute out-of-sample errors on each of the $G = 10$ test samples according to the likelihood-based score in equation (9). These errors on the test data are visualized in the right panel of Figure 8 with CGGM on the horizontal axis and TAGL on the vertical axis. For each of the test samples (dots), CGGM has a lower error thereby indicating that the more unbalanced cluster structure forms a better description of the conditional dependency structure in this context.

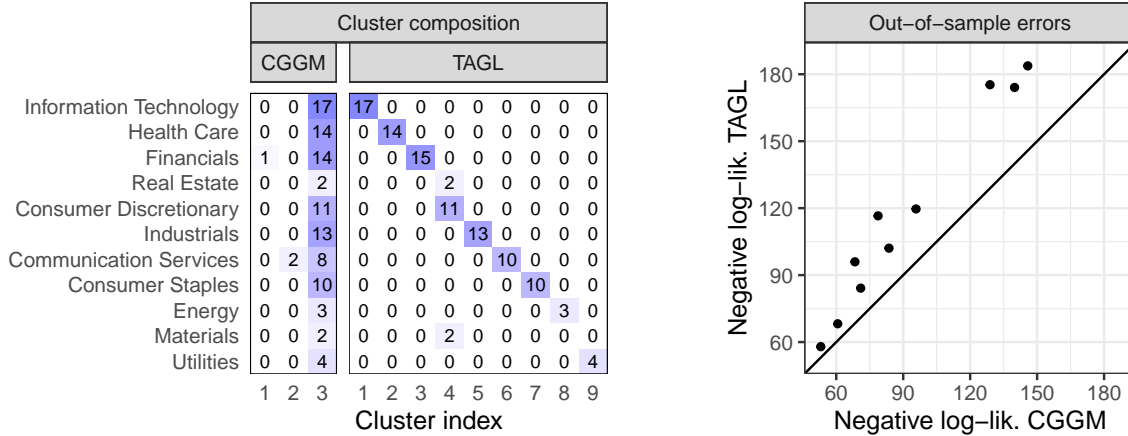


Figure 8: Finance application. Distribution of the sectors over the $K = 3$ cluster solution of CGGM and the $K = 9$ cluster solution of TAGL (left). Out-of-sample errors across the ten replications (dots) for CGGM versus TAGL (right).

5.2 OECD Well-Being Indicators

The second data set we analyze is one on OECD well-being indicators, collected during 2018. These data were previously analyzed in Cavicchia et al. (2022), and we acknowledge the authors for providing us with data access. The data contain $p = 11$ variables related to well-being: education, jobs, income, safety, health, environment, civic engagement, accessibility to services, housing, community, and life satisfaction, on which $n = 36$ countries are given a score ranging from 0 to 10. Note, however, that we split the sample of countries into two groups since Cavicchia et al. (2022) have found evidence for two groups of countries ($n_1 = 21$ and $n_2 = 14$) with distinct clustering structures.³

This application highlights the capabilities of CGGM in estimating a cluster hierarchy on the standardized well-being data. We thus report the whole clusterpath solution obtained by applying CGGM to estimate the precision matrix with different values of the tuning parameter λ for the two country groups. Moreover, due to the small sample sizes in both groups, we do not use cross-validation to select the tuning parameters ϕ and k for the weight matrix but use fixed values based on existing conventions instead, namely $\phi = 0.5$ and $k = 3$ (see e.g., Chi & Lange, 2015; Sun et al., 2021; Wang et al., 2018). Since our primary interest is in the clusterpaths, the refitting step described in Section 2.3.4 is not required as it would not affect

³The first group consists of the countries Australia, Austria, Belgium, Canada, Denmark, Finland, France, Germany, Iceland, Ireland, Italy, Japan, Luxembourg, Netherlands, New Zealand, Norway, Spain, Sweden, Switzerland, United Kingdom, United States, the second group consists of the countries Chile, Czech Republic, Estonia, Greece, Hungary, Israel, Korea, Latvia, Lithuania, Mexico, Poland, Portugal, Slovak Republic, Slovenia, Turkey. In our analysis, we omit Lithuania from the second group due to a missing value, hence $n_1 = 21$ and $n_2 = 14$.

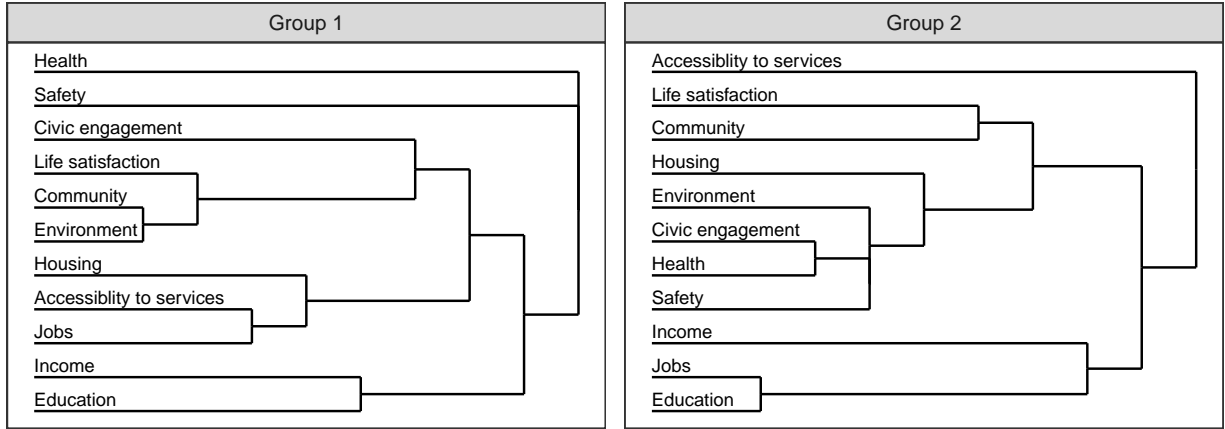


Figure 9: Well-being application. Clusterpath dendrograms obtained by CGGM on the two groups of countries.

the obtained paths. Figure 9 visualizes the dendrograms for the two groups of countries as obtained from CGGM’s complete clusterpath solution ranging from $p = 11$ clusters to one.

The analysis of well-being indicators across the two groups of countries reveals distinct clustering patterns that reflect their differing levels of development. In the first group (e.g., Australia, France, Switzerland), the aggregation of civic engagement, life satisfaction, community, environment, housing, accessibility to services, and jobs appears to reflect the social and environmental dimensions of well-being. Conversely, in the second group (e.g., Chile, Hungary, Mexico), safety and health are combined with the variables representing social and environmental dimensions, possibly suggesting a greater reliance on the community for these services. This contrasts with more developed countries where such services may be perceived as more self-evident. Additionally, in the second group, income, jobs, and education are grouped together, reflecting their importance to socioeconomic progress. Finally, note that we use CGGM with the precision matrix as object of interest; its block structure directly transfers to the covariance matrix thereby making our results comparable to those obtained in Cavicchia et al. (2022), who estimate the clustering structure on the covariance matrix.

5.3 Humor Styles Questionnaire

In surveys in the behavioral sciences, multiple rating-scale items are typically used to measure each latent construct of interest. For further analysis, it is common practice to compute mean scores across the respective items as measurements of each latent construct, which implies the assumption that the covariance matrix of the questionnaire items follows a block structure. The humor styles questionnaire (HSQ) developed by Martin et al. (2003) measures four latent constructs corresponding to different styles of humor: *affiliative*, *self-*

	Cluster 1	Cluster 2	Cluster 3	Cluster 4
Affiliative	{1, 5, 9, 13, 17, 21, 25, 29}			
Self-enhancing	{6, 30}	{2, 10, 14, 18, 22, 26}		
Aggressive			{3, 7, 11, 15, 19, 23, 27, 31}	
Self-defeating		{28}		{4, 8, 12, 16, 20, 24, 32}

Table 1: Humor styles questionnaire application. Allocation of the items developed by Martin et al. (2003) for measuring the four humor styles (in rows) to the four clusters found by CGGM for clustering the covariance matrix (in columns).

enhancing, *aggressive*, and *self-defeating*, with each construct being measured by eight items. An overview of the items is presented in Table 2 in Appendix D. If we can retrieve these four clusters of items in the covariance matrix, the assumption behind computing mean scores can be considered reasonable. We use responses to the HSQ on a five-point rating scale (anchored by 1 = “never or very rarely true” to 5 = “very often or always true”), which we obtained from https://openpsychometrics.org/_rawdata/. In addition to the aforementioned $p = 32$ items, participants were asked at the end of the questionnaire to indicate the accuracy of their responses. We restrict our analysis to participants who reported that their responses are fully accurate, and after removing 9 observations with missing responses, we retain $n = 182$ respondents.

Using 5-fold cross-validation, we apply the CGGM algorithm for clustering the covariance matrix (including the parameter re-estimation step) with a grid of $\phi \in \{1, 1.5, 2, 2.5, 3\}$ and $k \in \{1, 2, 3, 4, 5\}$ for the weight matrix. We obtain four clusters of items that largely overlap with the grouping of Martin et al. (2003), as shown in Table 1. Looking at the wording of the questionnaire items, the clustering found by CGGM is intuitive. All items of the *affiliative* group, which CGGM places in Cluster 1, refer to humor in social settings. In addition, the two items of the *self-enhancing* group that complete Cluster 1—items 6 and 30—address being alone as opposed to being with people. On the other hand, the remaining six items of the *self-enhancing* group, which CGGM puts in Cluster 2, all refer to using humor for dealing with feeling depressed, upset, unhappy, sad, or having problems. Item 28 from the *self-defeating* group, which completes Cluster 2, also addresses having problems or feeling unhappy. In contrast, the other seven items of this group, which form Cluster 4 in the CGGM solution, refer to laughing or letting others laugh at oneself. Finally, all items from the *aggressive* group address teasing and offensive or inappropriate humor, and are placed in Cluster 3 by CGGM.

Although the above interpretation of the obtained clusters is subjective, our findings suggest that the survey design of the HSQ may require further finetuning. Moreover, if subsequent analysis is based on mean scores, a slightly different allocation of the items to the latent constructs—the humor styles—may be more in line with the implicit assumption of a block structure in the covariance matrix.

6 Conclusion

We introduce a novel method to estimate Gaussian graphical models (GGMs) subject to node-clustering. Our method, which we call CGGM, uses a clusterpath penalty to produce a hierarchical clustering of variables (nodes in the graph) without relying on pre-existing notions of the cluster composition. An R package called `CGGMR` implements the proposed method and is available on the GitHub page of the first author.

In a comprehensive simulation study covering a wide range of graph structures, we compare CGGM to similar benchmarks such as TAGL and ComGGL. CGGM oftentimes surpasses the benchmarks both in terms of estimation accuracy and clustering performance, though the latter requires a refitting step particularly in noisy simulation designs. Through a diverse set of applications, we also demonstrate the versatility of CGGM in (i) learning cluster hierarchies in a fully data-driven way as compared to other benchmarks such as TAGL that require additional side-information for this task, (ii) delivering accurate cluster hierarchies that are transferable between the precision matrix and covariance matrix, and (iii) directly estimating clustered covariance matrices if these are the primary object of interest.

Concerning future work, CGGM may be extended to partial correlation matrices instead of precision matrices as the object of study. In contrast to the graphical lasso (glasso; Friedman et al., 2008), Carter et al. (2024) apply the sparsity penalty to the elements of the partial correlation matrix and call their method the partial correlation glasso. As a result, the sparsity structure estimated by this method is invariant to scalar multiplication of the data. CGGM can also be modified to accommodate clustering based on the partial correlation matrix, but this comes at the cost of the convexity of the objective function as with the partial correlation glasso.

Computational Details

All computations were performed with R (R Core Team, 2024). *Replication files will be made publicly available upon acceptance and a link will be included here.*

Acknowledgments

Andreas Alfons is supported by a grant from the Dutch Research Council (NWO), research program Vidi, grant number VI.Vidi.195.141. Ines Wilms is supported by the same funding agency under grant number VI.Vidi.211.032.

References

- Ambroise, C., Chiquet, J., & Matias, C. (2009). Inferring sparse Gaussian graphical models with latent structure. *Electronic Journal of Statistics*, *3*, 205–238. doi: <https://doi.org/10.1214/08-EJS314>
- Archakov, I., & Hansen, P. R. (2022). A canonical representation of block matrices with applications to covariance and correlation matrices. *The Review of Economics and Statistics*, 1–39. doi: https://doi.org/10.1162/rest_a_01258
- Banerjee, O., El Ghaoui, L., & d’Aspremont, A. (2008). Model selection through sparse maximum likelihood estimation for multivariate Gaussian or binary data. *Journal of Machine Learning Research*, *9*, 485–516.
- Brownlees, C., Guðmundsson, G. S., & Lugosi, G. (2022). Community detection in partial correlation network models. *Journal of Business & Economic Statistics*, *40*(1), 216–226. doi: <https://doi.org/10.1080/07350015.2020.1798241>
- Bunea, F., Giraud, C., Luo, X., Royer, M., & Verzelen, N. (2020). Model assisted variable clustering: minimax-optimal recovery and algorithms. *Annals of Statistics*, *48*(1), 111–137. doi: <https://doi.org/10.1214/18-AOS1794>
- Cai, T., Liu, W., & Luo, X. (2011). A constrained ℓ_1 minimization approach to sparse precision matrix estimation. *Journal of the American Statistical Association*, *106*(494), 594–607. doi: <https://doi.org/10.1198/jasa.2011.tm10155>
- Cardoso, J. V. d. M., Ying, J., & Palomar, D. P. (2020). Algorithms for learning graphs in financial markets. *arXiv preprint arXiv:2012.15410*. doi: <https://doi.org/10.48550/arXiv.2012.15410>
- Carter, J. S., Rossell, D., & Smith, J. Q. (2024). Partial correlation graphical lasso. *Scandinavian Journal of Statistics*, *51*(1), 32–63. doi: <https://doi.org/10.1111/sjos.12675>
- Cavicchia, C., Vichi, M., & Zaccaria, G. (2022). Gaussian mixture model with an extended ultrametric covariance structure. *Advances in Data Analysis and Classification*, *16*(2), 399–427. doi: <https://doi.org/10.1007/s11634-021-00488-x>

- Chi, E. C., Allen, G. I., & Baraniuk, R. G. (2017). Convex biclustering. *Biometrics*, *73*(1), 10–19. doi: <https://doi.org/10.1111/biom.12540>
- Chi, E. C., & Lange, K. L. (2015). Splitting methods for convex clustering. *Journal of Computational and Graphical Statistics*, *24*(4), 994–1013. doi: <https://doi.org/10.1080/10618600.2014.948181>
- Corsi, F. (2009). A simple approximate long-memory model of realized volatility. *Journal of Financial Econometrics*, *7*(2), 174–196. doi: <https://doi.org/10.1093/jjfinec/nbp001>
- Danaher, P., Wang, P., & Witten, D. M. (2014). The joint graphical lasso for inverse covariance estimation across multiple classes. *Journal of the Royal Statistical Society: Series B*, *76*(2), 373. doi: <https://doi.org/10.1111/rssb.12033>
- Duchi, J., Gould, S., & Koller, D. (2008). Projected subgradient methods for learning sparse Gaussians. In *Proceedings of the twenty-fourth conference on uncertainty in artificial intelligence* (pp. 153–160).
- Eisenach, C., Bunea, F., Ning, Y., & Dinicu, C. (2020). High-dimensional inference for cluster-based graphical models. *Journal of Machine Learning Research*, *21*(53), 1–55.
- Friedman, J., Hastie, T., & Tibshirani, R. (2008). Sparse inverse covariance estimation with the graphical lasso. *Biostatistics*, *9*(3), 432–441. doi: <https://doi.org/10.1093/biostatistics/kxm045>
- Gao, C., Zhu, Y., Shen, X., & Pan, W. (2016). Estimation of multiple networks in Gaussian mixture models. *Electronic Journal of Statistics*, *10*(1), 1133–1154. doi: <https://doi.org/10.1214/16-EJS1135>
- Gheche, M. E., & Frossard, P. (2020). Multilayer clustered graph learning. *arXiv preprint arXiv:2010.15456*. doi: <https://doi.org/10.48550/arXiv.2010.15456>
- Gower, J. C., & Groenen, P. J. F. (1991). Applications of the modified Leverrier-Faddeev algorithm for the construction of explicit matrix decompositions and inverses. *Utilitas Mathematica*, *40*, 51–64.
- Grechkin, M., Fazel, M., Witten, D., & Lee, S.-I. (2015). Pathway graphical lasso. In *Proceedings of the AAAI Conference on Artificial Intelligence* (Vol. 29). doi: <https://doi.org/10.1609/aaai.v29i1.9636>
- Hao, B., Sun, W. W., Liu, Y., & Cheng, G. (2018). Simultaneous clustering and estimation of heterogeneous graphical models. *Journal of Machine Learning Research*, *18*(217), 1–58.
- Heinävaara, O., Leppä-Aho, J., Corander, J., & Honkela, A. (2016). On the inconsistency of ℓ_1 -penalised sparse precision matrix estimation. *BMC Bioinformatics*, *17*(16), 99–107. doi: <https://doi.org/10.1186/s12859-016-1309-x>

- Hocking, T. D., Joulin, A., Bach, F., & Vert, J.-P. (2011). Clusterpath: An algorithm for clustering using convex fusion penalties. In *The 28th International Conference on Machine Learning*. Bellevue, Washington.
- Hosseini, M. J., & Lee, S.-I. (2016). Learning sparse Gaussian graphical models with overlapping blocks. In *Advances in Neural Information Processing Systems* (Vol. 29).
- Hubert, L., & Arabie, P. (1985). Comparing partitions. *Journal of Classification*, 2(1), 193–218. doi: <https://doi.org/10.1007/BF01908075>
- Kruskal, J. B. (1956). On the shortest spanning subtree of a graph and the traveling salesman problem. *Proceedings of the American Mathematical Society*, 7(1), 48–50.
- Kumar, S., Ying, J., De M. Cardoso, J. V., & Palomar, D. P. (2020). A unified framework for structured graph learning via spectral constraints. *Journal of Machine Learning Research*, 21(1), 1–60.
- Lindsten, F., Ohlsson, H., & Ljung, L. (2011). *Just relax and come clustering!: A convexification of k-means clustering* (Tech. Rep.). Linköping, Sweden: Department of Electrical Engineering, Linköping University.
- Marlin, B. M., & Murphy, K. P. (2009). Sparse Gaussian graphical models with unknown block structure. In *Proceedings of the 26th Annual International Conference on Machine Learning* (pp. 705–712). doi: <https://doi.org/10.1145/1553374.1553465>
- Martin, R. A., Puhlik-Doris, P., Larsen, G., Gray, J., & Weir, K. (2003). Individual differences in uses of humor and their relation to psychological well-being: Development of the humor styles questionnaire. *Journal of Research in Personality*, 37(1), 48–75. doi: [https://doi.org/10.1016/S0092-6566\(02\)00534-2](https://doi.org/10.1016/S0092-6566(02)00534-2)
- Martins, A. M. (2023). Stock market effects of silicon valley bank and credit suisse failure: Evidence for a sample of European listed banks. *Finance Research Letters*, 58, 104296. doi: <https://doi.org/10.1016/j.frl.2023.104296>
- Meinshausen, N., & Bühlmann, P. (2006). High-dimensional graphs and variable selection with the lasso. *The Annals of Statistics*, 34(3), 1436–1462. doi: <https://doi.org/10.1214/009053606000000281>
- Millington, T., & Niranjana, M. (2019). Quantifying influence in financial markets via partial correlation network inference. In *2019 11th International Symposium on Image and Signal Processing and Analysis (ISPA)* (pp. 306–311). doi: <https://doi.org/10.1109/ISPA.2019.8868437>
- Mohan, K., London, P., Fazel, M., Witten, D., & Lee, S.-I. (2014). Node-based learning of multiple Gaussian graphical models. *Journal of Machine Learning Research*, 15(1), 445–488.

- Nie, F., Wang, X., Jordan, M., & Huang, H. (2016). The constrained Laplacian rank algorithm for graph-based clustering. In *Proceedings of the AAAI Conference on Artificial Intelligence* (Vol. 30). doi: <https://doi.org/10.1609/aaai.v30i1.10302>
- Parkinson, M. (1980). The extreme value method for estimating the variance of the rate of return. *Journal of Business*, 53(1), 61–65.
- Pelckmans, K., De Brabanter, J., Suykens, J. A. K., & de Moor, B. (2005). Convex clustering shrinkage. In *PASCAL Workshop on Statistics and Optimization of Clustering Workshop*.
- Peng, J., Wang, P., Zhou, N., & Zhu, J. (2009). Partial correlation estimation by joint sparse regression models. *Journal of the American Statistical Association*, 104(486), 735–746. doi: <https://doi.org/10.1198/jasa.2009.0126>
- Pircalabelu, E., & Claeskens, G. (2020). Community-based group graphical lasso. *Journal of Machine Learning Research*, 21(1), 1–32.
- R Core Team. (2024). R: A language and environment for statistical computing [Computer software manual]. Vienna, Austria. Retrieved from <https://www.R-project.org/>
- Rothman, A. J., Bickel, P. J., Levina, E., & Zhu, J. (2008). Sparse permutation invariant covariance estimation. *Electronic Journal of Statistics*, 2, 494–515. doi: <https://doi.org/10.1214/08-EJS176>
- Schmidt, M., Berg, E., Friedlander, M., & Murphy, K. (2009). Optimizing costly functions with simple constraints: A limited-memory projected quasi-newton algorithm. In *Proceedings of the Twelfth International Conference on Artificial Intelligence and Statistics* (Vol. 5, pp. 456–463).
- Shi, D., Wang, T., & Ying, Z. (2024). Simultaneous identification of sparse structures and communities in heterogeneous graphical models. *arXiv preprint arXiv:2405.09841*. doi: <https://doi.org/10.48550/arXiv.2405.09841>
- Sun, D., Toh, K.-C., & Yuan, Y. (2021). Convex clustering: Model, theoretical guarantee and efficient algorithm. *Journal of Machine Learning Research*, 22(9), 1–32.
- Tan, K. M., Witten, D., & Shojaie, A. (2015). The cluster graphical lasso for improved estimation of Gaussian graphical models. *Computational Statistics & Data Analysis*, 85, 23–36. doi: <https://doi.org/10.1016/j.csda.2014.11.015>
- Tarzanagh, D. A., Balzano, L., & Hero, A. O. (2021). Fair structure learning in heterogeneous graphical models. *arXiv preprint arXiv:2112.05128*. doi: <https://doi.org/10.48550/arXiv.2112.05128>

- Tarzanagh, D. A., & Michailidis, G. (2018). Estimation of graphical models through structured norm minimization. *Journal of Machine Learning Research*, 18(1), 1–48.
- Touw, D. J. W., Groenen, P. J. F., & Terada, Y. (2022). Convex clustering through MM: An efficient algorithm to perform hierarchical clustering. *arXiv preprint arXiv:2211.01877*. doi: <https://doi.org/10.48550/arXiv.2211.01877>
- Wang, B., Zhang, Y., Sun, W. W., & Fang, Y. (2018). Sparse convex clustering. *Journal of Computational and Graphical Statistics*, 27(2), 393–403. doi: <https://doi.org/10.1080/10618600.2017.1377081>
- Wilms, I., & Bien, J. (2022). Tree-based node aggregation in sparse graphical models. *Journal of Machine Learning Research*, 23(243), 1–36.
- Yao, T., & Allen, G. I. (2019). Clustered Gaussian graphical model via symmetric convex clustering. In *2019 IEEE Data Science Workshop (DSW)* (pp. 76–82). doi: <https://doi.org/10.1109/DSW.2019.8755774>
- Yuan, M. (2010). High dimensional inverse covariance matrix estimation via linear programming. *Journal of Machine Learning Research*, 11(79), 2261–2286.
- Yuan, M., & Lin, Y. (2006). Model selection and estimation in regression with grouped variables. *Journal of the Royal Statistical Society: Series B*, 68(1), 49–67. doi: <https://doi.org/10.1111/j.1467-9868.2005.00532.x>
- Yuan, M., & Lin, Y. (2007). Model selection and estimation in the Gaussian graphical model. *Biometrika*, 94(1), 19–35. doi: <https://doi.org/10.1093/biomet/asm018>

A Derivations Clusterpath Estimator

The main purpose of re-expressing the objective function $L(\Theta)$ in terms of \mathbf{A} and \mathbf{R} is to obtain a more compact expression that permits straightforward updates for solving optimization problem (1). To this end, we begin by defining the key variables and then work our way through the different terms of the objective function (3).

For any number of clusters $1 \leq K \leq p$, the precision matrix contains the block-structure

$$\Theta = \begin{bmatrix} (a_{11} - r_{11})\mathbf{I} + r_{11}\mathbf{1}\mathbf{1}^\top & r_{12}\mathbf{1}\mathbf{1}^\top & \cdots & r_{1K}\mathbf{1}\mathbf{1}^\top \\ r_{21}\mathbf{1}\mathbf{1}^\top & (a_{22} - r_{22})\mathbf{I} + r_{22}\mathbf{1}\mathbf{1}^\top & \cdots & r_{2K}\mathbf{1}\mathbf{1}^\top \\ \vdots & \vdots & \ddots & \vdots \\ r_{K1}\mathbf{1}\mathbf{1}^\top & r_{K2}\mathbf{1}\mathbf{1}^\top & \cdots & (a_{KK} - r_{KK})\mathbf{I} + r_{KK}\mathbf{1}\mathbf{1}^\top \end{bmatrix}.$$

Without loss of generality, we assume that the variables have been reordered such that those in cluster 1 form the first block, those in cluster 2 the second block, and so on. Let \mathbf{U} be the $p \times K$ membership matrix with $u_{jk} = 1$ if variable j belongs to cluster k and zero otherwise. Then, $\mathbf{P} = \mathbf{U}^\top \mathbf{U}$ is the diagonal matrix with the number of variables p_k per cluster as diagonal elements and $\mathbf{p} = \mathbf{1}^\top \mathbf{U}$ is the $K \times 1$ vector with elements p_k . It can be verified that $\mathbf{X}\mathbf{U}\mathbf{P}^{-1}$ computes the cluster averages of the original variables in \mathbf{X} .

First, we focus on the first term in objective function (3), the log determinant of Θ , to obtain a convenient expression in \mathbf{A} and \mathbf{R} . We show that Θ can be split in a linear space that depends on \mathbf{A} and \mathbf{R} and an orthogonal linear space that is only dependent on the diagonal blocks of Θ and thus on \mathbf{A} and the diagonal elements of \mathbf{R} . To do so, we first consider what happens if we take cluster averages, that is,

$$\begin{aligned} \mathbf{P}^{-1}\mathbf{U}^\top \Theta \mathbf{U}\mathbf{P}^{-1} &= \mathbf{P}^{-1}\mathbf{U}^\top \left(\mathbf{U}\mathbf{R}\mathbf{U}^\top + \begin{bmatrix} (a_{11} - r_{11})\mathbf{I} & \mathbf{0} & \cdots & \mathbf{0} \\ \mathbf{0} & (a_{22} - r_{22})\mathbf{I} & \cdots & \mathbf{0} \\ \vdots & \vdots & \ddots & \vdots \\ \mathbf{0} & \mathbf{0} & \cdots & (a_{KK} - r_{KK})\mathbf{I} \end{bmatrix} \right) \mathbf{U}\mathbf{P}^{-1} \\ &= \mathbf{R} + \mathbf{P}^{-1} \begin{bmatrix} (a_{11} - r_{11}) & 0 & \cdots & 0 \\ 0 & (a_{22} - r_{22}) & \cdots & 0 \\ \vdots & \vdots & \ddots & \vdots \\ 0 & 0 & \cdots & (a_{KK} - r_{KK}) \end{bmatrix} \\ &= \mathbf{R} + \begin{bmatrix} (a_{11} - r_{11})/p_1 & 0 & \cdots & 0 \\ 0 & (a_{22} - r_{22})/p_2 & \cdots & 0 \\ \vdots & \vdots & \ddots & \vdots \\ 0 & 0 & \cdots & (a_{KK} - r_{KK})/p_{KK} \end{bmatrix} \\ &= \mathbf{R}^*. \end{aligned}$$

Then,

$$\mathbf{UR}^*\mathbf{U}^\top = \begin{bmatrix} r_{11}^*\mathbf{1}\mathbf{1}^\top & r_{12}\mathbf{1}\mathbf{1}^\top & \cdots & r_{1K}\mathbf{1}\mathbf{1}^\top \\ r_{21}\mathbf{1}\mathbf{1}^\top & r_{22}^*\mathbf{1}\mathbf{1}^\top & \cdots & r_{2K}\mathbf{1}\mathbf{1}^\top \\ \vdots & \vdots & \ddots & \vdots \\ r_{K1}\mathbf{1}\mathbf{1}^\top & r_{K2}\mathbf{1}\mathbf{1}^\top & \cdots & r_{KK}^*\mathbf{1}\mathbf{1}^\top \end{bmatrix},$$

where $r_{kk}^* = (a_{kk} - r_{kk})/p_k + r_{kk}$ so that $\Theta - \mathbf{UR}^*\mathbf{U}^\top$ has off-diagonal blocks equal to zero and diagonal blocks equal to $(a_{kk} - r_{kk})(\mathbf{I} - p_k^{-1}\mathbf{1}\mathbf{1}^\top) = (a_{kk} - r_{kk})\mathbf{J}_k$ with \mathbf{J}_k the $p_k \times p_k$ centering matrix. This yields

$$\Theta = \mathbf{UR}^*\mathbf{U}^\top + \begin{bmatrix} (a_{11} - r_{11})\mathbf{J}_1 & \mathbf{0} & \cdots & \mathbf{0} \\ \mathbf{0} & (a_{22} - r_{22})\mathbf{J}_2 & \cdots & \mathbf{0} \\ \vdots & \vdots & \ddots & \vdots \\ \mathbf{0} & \mathbf{0} & \cdots & (a_{KK} - r_{KK})\mathbf{J}_K \end{bmatrix}, \quad (10)$$

as also displayed in (4). It can be verified that this decomposition is indeed orthogonal because post-multiplying the final term with \mathbf{U} yields zero due to the centering matrices.

Next, it is well known that the determinant is equal to the product of the eigenvalues of the matrix. Therefore, we require the eigenvalues of both parts of decomposition (10). Let the eigendecomposition of Θ be given by

$$\begin{aligned} \Theta &= \mathbf{Q}\mathbf{\Gamma}\mathbf{Q}^\top \\ &= \mathbf{Q}_1\mathbf{\Gamma}_1\mathbf{Q}_1^\top + \mathbf{Q}_2\mathbf{\Gamma}_2\mathbf{Q}_2^\top \\ &= \mathbf{UR}^*\mathbf{U}^\top + \begin{bmatrix} (a_{11} - r_{11})\mathbf{J}_1 & \mathbf{0} & \cdots & \mathbf{0} \\ \mathbf{0} & (a_{22} - r_{22})\mathbf{J}_2 & \cdots & \mathbf{0} \\ \vdots & \vdots & \ddots & \vdots \\ \mathbf{0} & \mathbf{0} & \cdots & (a_{KK} - r_{KK})\mathbf{J}_K \end{bmatrix}. \end{aligned}$$

We now need to find $\mathbf{\Gamma}_1$ in the eigendecomposition $\mathbf{UR}^*\mathbf{U}^\top = \mathbf{Q}_1\mathbf{\Gamma}_1\mathbf{Q}_1^\top$. Pre- and post-multiplying with an orthonormal matrix does not change the eigenvalues. A convenient orthonormal matrix for pre-multiplication is therefore $\mathbf{P}^{-1/2}\mathbf{U}$ giving

$$\begin{aligned} \mathbf{UR}^*\mathbf{U}^\top &= \mathbf{Q}_1\mathbf{\Gamma}_1\mathbf{Q}_1^\top \\ \mathbf{P}^{-1/2}\mathbf{U}^\top\mathbf{UR}^*\mathbf{U}^\top\mathbf{U}\mathbf{P}^{-1/2} &= \mathbf{P}^{-1/2}\mathbf{U}^\top\mathbf{Q}_1\mathbf{\Gamma}_1\mathbf{Q}_1^\top\mathbf{U}\mathbf{P}^{-1/2} \\ \mathbf{P}^{1/2}\mathbf{R}^*\mathbf{P}^{1/2} &= \mathbf{Q}_1^*\mathbf{\Gamma}_1\mathbf{Q}_1^{*\top} \\ \begin{bmatrix} p_1r_{11}^* & (p_1p_2)^{1/2}r_{12} & \cdots & (p_1p_K)^{1/2}r_{1K} \\ (p_1p_2)^{1/2}r_{21} & p_2r_{22}^* & \cdots & (p_2p_K)^{1/2}r_{2K} \\ \vdots & \vdots & \ddots & \vdots \\ (p_1p_K)^{1/2}r_{K1} & (p_2p_K)^{1/2}r_{K2} & \cdots & p_Kr_{KK}^* \end{bmatrix} &= \mathbf{Q}_1^*\mathbf{\Gamma}_1\mathbf{Q}_1^{*\top}, \end{aligned}$$

which shows that in the case of K clusters, the eigenvalues corresponding to the space spanned by \mathbf{R}^* in decomposition (10) can be obtained by considering the eigenvalues of a $K \times K$ matrix.

The second part of the space in decomposition (10) is spanned by the diagonal centering matrices $(a_{kk} - r_{kk})\mathbf{J}_k$. The centering matrix is a projector matrix that has $p_k - 1$ eigenvalues of 1, so that $(a_{kk} - r_{kk})\mathbf{J}_k$ has $p_k - 1$ eigenvalues of $a_{kk} - r_{kk}$.

Combining both parts, we can express

$$-\log |\Theta| = -\log |\mathbf{P}^{1/2}\mathbf{R}^*\mathbf{P}^{1/2}| - \sum_{k=1}^K (p_k - 1) \log(a_{kk} - r_{kk}).$$

Second, we address the second term in objective function (3), the trace of the matrix product $\mathbf{S}\Theta$. It is straightforward to express this term in terms of \mathbf{A} and \mathbf{R} , namely

$$\text{tr } \mathbf{S}\Theta = \text{tr } \mathbf{S}\mathbf{U}\mathbf{R}\mathbf{U}^\top + \sum_{\ell=1}^K (a_{\ell\ell} - r_{\ell\ell}) \text{tr } \mathbf{S}_\ell,$$

where \mathbf{S}_ℓ is the sample covariance matrix computed from the p_ℓ variables in cluster ℓ .

Third, the clusterpath penalty term in objective function (3) can be written as

$$\mathcal{P}(\Theta) = \sum_{j < j'} w_{jj'} d_{jj'}(\Theta) = \sum_{k < \ell} \sum_{j \in \mathcal{C}_k} \sum_{j' \in \mathcal{C}_\ell} w_{jj'} d_{jj'}(\Theta),$$

where \mathcal{C}_k denotes the set of variables belonging to cluster k . Because $d_{jj'}(\Theta)$ evaluates to the same value for all $j \in \mathcal{C}_k$ and $j' \in \mathcal{C}_\ell$, the penalty can be further reduced into

$$\mathcal{P}(\Theta) = \sum_{k < \ell} \left(\sum_{j \in \mathcal{C}_k} \sum_{j' \in \mathcal{C}_\ell} w_{jj'} \right) d_{k\ell}(\mathbf{A}, \mathbf{R}) = \sum_{k < \ell} \mathbf{u}_k^\top \mathbf{W} \mathbf{u}_\ell d_{k\ell}(\mathbf{A}, \mathbf{R}),$$

where \mathbf{W} is the symmetric $p \times p$ weight matrix containing the individual weights $w_{jj'}$, \mathbf{u}_k denotes the k^{th} column of the membership matrix \mathbf{U} , and

$$d_{k\ell}^2(\mathbf{A}, \mathbf{R}) = (a_{kk} - a_{\ell\ell})^2 + (p_k - 1)(r_{kk} - r_{k\ell})^2 + (p_\ell - 1)(r_{\ell\ell} - r_{k\ell})^2 + \sum_{\substack{m=1 \\ m \notin \{k, \ell\}}}^K p_m (r_{km} - r_{\ell m})^2.$$

Note that the subscripts $k\ell$ in $d_{k\ell}(\mathbf{A}, \mathbf{R})$ always refer to the cluster formulation of the Euclidean distance.

Finally, combining all decomposed terms we obtain expression (5) for the objective function $L(\Theta)$ in terms of \mathbf{A} and \mathbf{R} , namely

$$\begin{aligned} L(\Theta) &= L(\mathbf{A}, \mathbf{R}) \\ &= -\log |\mathbf{P}^{1/2}\mathbf{R}^*\mathbf{P}^{1/2}| - \sum_{k=1}^K (p_k - 1) \log(a_{kk} - r_{kk}) + \text{tr } \mathbf{S}\mathbf{U}\mathbf{R}\mathbf{U}^\top + \sum_{\ell=1}^K (a_{\ell\ell} - r_{\ell\ell}) \text{tr } \mathbf{S}_\ell \\ &\quad + \lambda \sum_{k < \ell} \mathbf{u}_k^\top \mathbf{W} \mathbf{u}_\ell d_{k\ell}(\mathbf{A}, \mathbf{R}). \end{aligned}$$

B Derivations Cyclic Block Coordinate Descent Algorithm

We provide detailed derivations of the parameterization of the objective function in Appendix B.1 and its gradient and Hessian in Appendix B.2.

B.1 Parameterization

In Section 2.2, efficient expressions have been obtained that make use of the block structure of Θ . What remains to be done is to separate $L(\mathbf{A}, \mathbf{R})$ into those parts that depend on cluster k and those that do not. In the following, we make the assumption, without loss of generality, that the variables are arranged to consistently position cluster k as the last cluster. Let the elements of Θ that pertain to cluster k be separated from the others (denoted by the subscript 0), so that

$$\Theta = \left[\begin{array}{ccc|c} (a_{11} - r_{11})\mathbf{I} + r_{11}\mathbf{1}\mathbf{1}^\top & r_{12}\mathbf{1}\mathbf{1}^\top & \cdots & r_{13}\mathbf{1}\mathbf{1}^\top \\ r_{21}\mathbf{1}\mathbf{1}^\top & (a_{22} - r_{22})\mathbf{I} + r_{22}\mathbf{1}\mathbf{1}^\top & \cdots & r_{2k}\mathbf{1}\mathbf{1}^\top \\ \vdots & \vdots & \ddots & \vdots \\ \hline r_{k1}\mathbf{1}\mathbf{1}^\top & r_{k2}\mathbf{1}\mathbf{1}^\top & \cdots & (a_{kk} - r_{kk})\mathbf{I} + r_{kk}\mathbf{1}\mathbf{1}^\top \end{array} \right]$$

$$= \left[\begin{array}{c|c} \Theta_0 & \Theta_{0k} \\ \hline \Theta_{0k}^\top & \Theta_{kk} \end{array} \right].$$

Consequently, updating all parameters in \mathbf{A} and \mathbf{R} that are associated with cluster k updates an entire block of variables in Θ . To separate the term $-\log |\mathbf{P}^{1/2}\mathbf{R}^*\mathbf{P}^{1/2}|$ in objective function (5), it helps to write $\mathbf{P}^{1/2}\mathbf{R}^*\mathbf{P}^{1/2}$ as the 2×2 block matrix

$$\mathbf{P}^{1/2}\mathbf{R}^*\mathbf{P}^{1/2} = \left[\begin{array}{c|c} \mathbf{P}_0^{1/2}\mathbf{R}_0^*\mathbf{P}_0^{1/2} & p_k^{1/2}\mathbf{P}_0^{1/2}\mathbf{r}_k \\ \hline p_k^{1/2}(\mathbf{P}_0^{1/2}\mathbf{r}_k)^\top & p_k r_{kk}^* \end{array} \right]$$

with \mathbf{r}_k the $K - 1$ vector containing all elements in the k^{th} column of \mathbf{R} apart from r_{kk} , and

$$\mathbf{P} = \left[\begin{array}{cc} \mathbf{P}_0 & \mathbf{0} \\ \mathbf{0}^\top & p_k \end{array} \right].$$

From linear algebra, we have the following expression for the log determinant of the 2×2 block matrix

$$-\log |\mathbf{P}^{1/2}\mathbf{R}^*\mathbf{P}^{1/2}| = -\log |\mathbf{P}_0^{1/2}\mathbf{R}_0^*\mathbf{P}_0^{1/2}| - \log(a_{kk} + (p_k - 1)r_{kk} - p_k\mathbf{r}_k^\top(\mathbf{R}_0^*)^{-1}\mathbf{r}_k).$$

This allows us to rewrite the negative log determinant of Θ as

$$\begin{aligned} -\log |\Theta| &= -\log |\mathbf{P}_0^{1/2}\mathbf{R}_0^*\mathbf{P}_0^{1/2}| - \log(a_{kk} + (p_k - 1)r_{kk} - p_k\mathbf{r}_k^\top(\mathbf{R}_0^*)^{-1}\mathbf{r}_k) \\ &\quad - (p_k - 1) \log(a_{kk} - r_{kk}) - \sum_{\substack{\ell=1 \\ \ell \neq k}}^K (p_\ell - 1) \log(a_{\ell\ell} - r_{\ell\ell}). \end{aligned} \tag{11}$$

Using the re-expression from objective function (5), the trace of $\mathbf{S}\Theta$ separates readily into

$$\text{tr } \mathbf{S}\Theta = 2\mathbf{u}_k^\top \mathbf{S}\mathbf{U}_0 \mathbf{r}_k + \mathbf{u}_k^\top \mathbf{S}\mathbf{u}_k r_{kk} + (a_{kk} - r_{kk}) \text{tr } \mathbf{S}_k + \text{tr } \mathbf{S}\mathbf{U}_0 \mathbf{R}_0 \mathbf{U}_0^\top + \sum_{\substack{\ell=1 \\ \ell \neq k}}^K (a_{\ell\ell} - r_{\ell\ell}) \text{tr } \mathbf{S}_\ell.$$

It can be verified that the last two terms are constant in a_{kk} , \mathbf{r}_k , and r_{kk} , and the remaining terms are linear in these unknowns. Finally, due to the symmetry of \mathbf{R} , the clusterpath penalty is not separable into parts dependent and independent of cluster k .

Combining the foregoing results, $L(\mathbf{A}, \mathbf{R})$ can be expressed in terms of parts a_{kk} , \mathbf{r}_k , and r_{kk} , and we obtain $L(a_{kk}, \mathbf{r}_k, r_{kk})$ in equation (6) as

$$\begin{aligned} L(a_{kk}, \mathbf{r}_k, r_{kk}) &= L_{\text{det}}(a_{kk}, \mathbf{r}_k, r_{kk}) + L_{\text{cov}}(a_{kk}, \mathbf{r}_k, r_{kk}) + L_{\text{cpath}}(a_{kk}, \mathbf{r}_k, r_{kk}) + C \\ &= -\log(a_{kk} + (p_k - 1)r_{kk} - p_k \mathbf{r}_k^\top (\mathbf{R}_0^*)^{-1} \mathbf{r}_k) - (p_k - 1) \log(a_{kk} - r_{kk}) \\ &\quad + 2\mathbf{u}_k^\top \mathbf{S}\mathbf{U}_0 \mathbf{r}_k + \mathbf{u}_k^\top \mathbf{S}\mathbf{u}_k r_{kk} + (a_{kk} - r_{kk}) \text{tr } \mathbf{S}_k \\ &\quad + \lambda \left(\sum_{k < \ell} \mathbf{u}_k^\top \mathbf{W}\mathbf{u}_\ell d_{k\ell}(\mathbf{A}, \mathbf{R}) \right) + C \end{aligned}$$

with

$$\begin{aligned} C &= -\log |\mathbf{P}_0^{1/2} \mathbf{R}_0^* \mathbf{P}_0^{1/2}| - \sum_{\substack{\ell=1 \\ \ell \neq k}}^K (p_\ell - 1) \log(a_{\ell\ell} - r_{\ell\ell}) \\ &\quad + \text{tr } \mathbf{S}\mathbf{U}_0 \mathbf{R}_0 \mathbf{U}_0^\top + \sum_{\substack{\ell=1 \\ \ell \neq k}}^K (a_{\ell\ell} - r_{\ell\ell}) \text{tr } \mathbf{S}_\ell. \end{aligned}$$

B.2 Derivations of the Gradient and Hessian

In the derivations that follow, we obtain expressions for the gradient and Hessian of (6). To shorten notation, let $\mathbf{V} = (\mathbf{R}_0^*)^{-1}$ and

$$h(a_{kk}, \mathbf{r}_k, r_{kk}) = a_{kk} + (p_k - 1)r_{kk} - p_k \mathbf{r}_k^\top \mathbf{V} \mathbf{r}_k.$$

For convenience, the elements r_{km} of the vector \mathbf{r}_k are treated individually. Consequently, we should note that $1 \leq m \leq K$, $m \neq k$. For the gradient, we obtain

$$\begin{aligned} \frac{\partial L_{\text{det}}(a_{kk}, \mathbf{r}_k, r_{kk})}{\partial a_{kk}} &= -\frac{1}{h(a_{kk}, \mathbf{r}_k, r_{kk})} - \frac{p_k - 1}{a_{kk} - r_{kk}} \\ \frac{\partial L_{\text{det}}(a_{kk}, \mathbf{r}_k, r_{kk})}{\partial r_{km}} &= \frac{2p_k}{h(a_{kk}, \mathbf{r}_k, r_{kk})} \mathbf{v}_m^\top \mathbf{r}_k \\ \frac{\partial L_{\text{det}}(a_{kk}, \mathbf{r}_k, r_{kk})}{\partial r_{kk}} &= -\frac{p_k - 1}{h(a_{kk}, \mathbf{r}_k, r_{kk})} + \frac{p_k - 1}{a_{kk} - r_{kk}} \\ \frac{\partial L_{\text{cov}}(a_{kk}, \mathbf{r}_k, r_{kk})}{\partial a_{kk}} &= \text{tr } \mathbf{S}_k \\ \frac{\partial L_{\text{cov}}(a_{kk}, \mathbf{r}_k, r_{kk})}{\partial r_{km}} &= 2\mathbf{u}_m^\top \mathbf{S}\mathbf{u}_k \end{aligned}$$

$$\begin{aligned}
\frac{\partial L_{\text{cov}}(a_{kk}, \mathbf{r}_k, r_{kk})}{\partial r_{kk}} &= \mathbf{u}_k^\top \mathbf{S} \mathbf{u}_k - \text{tr} \mathbf{S}_k \\
\frac{\partial L_{\text{cpath}}(a_{kk}, \mathbf{r}_k, r_{kk})}{\partial a_{kk}} &= \lambda \sum_{\substack{\ell=1 \\ \ell \neq k}}^K \frac{\mathbf{u}_k^\top \mathbf{W} \mathbf{u}_\ell}{d_{k\ell}(\mathbf{A}, \mathbf{R})} (a_{kk} - a_{\ell\ell}) \\
\frac{\partial L_{\text{cpath}}(a_{kk}, \mathbf{r}_k, r_{kk})}{\partial r_{km}} &= \lambda \sum_{\substack{\ell=1 \\ \ell \notin \{k, m\}}}^K \left(\frac{\mathbf{u}_k^\top \mathbf{W} \mathbf{u}_\ell}{d_{k\ell}(\mathbf{A}, \mathbf{R})} p_m (r_{km} - r_{m\ell}) + \frac{\mathbf{u}_m^\top \mathbf{W} \mathbf{u}_\ell}{d_{m\ell}(\mathbf{A}, \mathbf{R})} p_k (r_{km} - r_{k\ell}) \right) \\
&\quad + \lambda \frac{\mathbf{u}_k^\top \mathbf{W} \mathbf{u}_m}{d_{km}(\mathbf{A}, \mathbf{R})} ((p_k - 1)(r_{km} - r_{kk}) + (p_m - 1)(r_{km} - r_{mm})) \\
\frac{\partial L_{\text{cpath}}(a_{kk}, \mathbf{r}_k, r_{kk})}{\partial r_{kk}} &= \lambda (p_k - 1) \sum_{\substack{\ell=1 \\ \ell \neq k}}^K \frac{\mathbf{u}_k^\top \mathbf{W} \mathbf{u}_\ell}{d_{k\ell}(\mathbf{A}, \mathbf{R})} (r_{kk} - r_{k\ell}).
\end{aligned}$$

In the derivations for the Hessian, we require an additional index m' to define the off-diagonal elements in the block $\partial^2 L(a_{kk}, \mathbf{r}_k, r_{kk}) / \partial \mathbf{r}_k^2$ that satisfies $1 \leq m' \leq K$, $m' \notin \{k, m\}$. For the Hessian, we obtain

$$\begin{aligned}
\frac{\partial^2 L_{\text{det}}(a_{kk}, \mathbf{r}_k, r_{kk})}{\partial a_{kk}^2} &= \frac{1}{h^2(a_{kk}, \mathbf{r}_k, r_{kk})} + \frac{p_k - 1}{(a_{kk} - r_{kk})^2} \\
\frac{\partial^2 L_{\text{det}}(a_{kk}, \mathbf{r}_k, r_{kk})}{\partial a_{kk} \partial r_{km}} &= -\frac{2p_k}{h^2(a_{kk}, \mathbf{r}_k, r_{kk})} \mathbf{v}_m^\top \mathbf{r}_k \\
\frac{\partial^2 L_{\text{det}}(a_{kk}, \mathbf{r}_k, r_{kk})}{\partial a_{kk} \partial r_{kk}} &= \frac{p_k - 1}{h^2(a_{kk}, \mathbf{r}_k, r_{kk})} - \frac{p_k - 1}{(a_{kk} - r_{kk})^2} \\
\frac{\partial^2 L_{\text{det}}(a_{kk}, \mathbf{r}_k, r_{km})}{\partial r_{km}^2} &= \frac{2p_k}{h(a_{kk}, \mathbf{r}_k, r_{kk})} v_{mm} + \frac{4p_k^2}{h^2(a_{kk}, \mathbf{r}_k, r_{kk})} \mathbf{v}_m^\top \mathbf{r}_k \mathbf{r}_k^\top \mathbf{v}_m \\
\frac{\partial^2 L_{\text{det}}(a_{kk}, \mathbf{r}_k, r_{km})}{\partial r_{km} \partial r_{km'}} &= \frac{2p_k}{h(a_{kk}, \mathbf{r}_k, r_{kk})} v_{mm'} + \frac{4p_k^2}{h^2(a_{kk}, \mathbf{r}_k, r_{kk})} \mathbf{v}_m^\top \mathbf{r}_k \mathbf{r}_k^\top \mathbf{v}_{m'} \\
\frac{\partial^2 L_{\text{det}}(a_{kk}, \mathbf{r}_k, r_{kk})}{\partial r_{km} \partial r_{kk}} &= -\frac{2p_k(p_k - 1)}{h^2(a_{kk}, \mathbf{r}_k, r_{kk})} \mathbf{v}_m^\top \mathbf{r}_k \\
\frac{\partial^2 L_{\text{det}}(a_{kk}, \mathbf{r}_k, r_{kk})}{\partial r_{kk}^2} &= \frac{(p_k - 1)^2}{h^2(a_{kk}, \mathbf{r}_k, r_{kk})} + \frac{p_k - 1}{(a_{kk} - r_{kk})^2} \\
\frac{\partial^2 L_{\text{cpath}}(a_{kk}, \mathbf{r}_k, r_{kk})}{\partial a_{kk}^2} &= \lambda \sum_{\substack{\ell=1 \\ \ell \neq k}}^K \mathbf{u}_k^\top \mathbf{W} \mathbf{u}_\ell \left(\frac{1}{d_{k\ell}(\mathbf{A}, \mathbf{R})} - \frac{(a_{kk} - a_{\ell\ell})^2}{d_{k\ell}^3(\mathbf{A}, \mathbf{R})} \right) \\
\frac{\partial^2 L_{\text{cpath}}(a_{kk}, \mathbf{r}_k, r_{kk})}{\partial a_{kk} \partial r_{km}} &= -\lambda \sum_{\substack{\ell=1 \\ \ell \notin \{k, m\}}}^K \frac{\mathbf{u}_k^\top \mathbf{W} \mathbf{u}_\ell}{d_{k\ell}^3(\mathbf{A}, \mathbf{R})} p_m (a_{kk} - a_{\ell\ell})(r_{km} - r_{m\ell}) \\
&\quad - \lambda \frac{\mathbf{u}_k^\top \mathbf{W} \mathbf{u}_m}{d_{km}^3(\mathbf{A}, \mathbf{R})} (a_{kk} - a_{mm}) ((p_k - 1)(r_{km} - r_{kk}) + (p_m - 1)(r_{km} - r_{mm})) \\
\frac{\partial^2 L_{\text{cpath}}(a_{kk}, \mathbf{r}_k, r_{kk})}{\partial a_{kk} \partial r_{kk}} &= -\lambda (p_k - 1) \sum_{\substack{\ell=1 \\ \ell \neq k}}^K \frac{\mathbf{u}_k^\top \mathbf{W} \mathbf{u}_\ell}{d_{k\ell}^3(\mathbf{A}, \mathbf{R})} (a_{kk} - a_{\ell\ell})(r_{kk} - r_{k\ell}) \\
\frac{\partial^2 L_{\text{cpath}}(a_{kk}, \mathbf{r}_k, r_{kk})}{\partial r_{km}^2} &= \lambda \sum_{\substack{\ell=1 \\ \ell \notin \{k, m\}}}^K p_m \frac{\mathbf{u}_k^\top \mathbf{W} \mathbf{u}_\ell}{d_{k\ell}(\mathbf{A}, \mathbf{R})} \left(1 - \frac{p_m (r_{km} - r_{m\ell})^2}{d_{k\ell}^2(\mathbf{A}, \mathbf{R})} \right)
\end{aligned}$$

$$\begin{aligned}
& + \lambda \sum_{\substack{\ell=1 \\ \ell \notin \{k,m\}}}^K p_k \frac{\mathbf{u}_m^\top \mathbf{W} \mathbf{u}_\ell}{d_{m\ell}(\mathbf{A}, \mathbf{R})} \left(1 - \frac{p_k (r_{km} - r_{k\ell})^2}{d_{m\ell}^2(\mathbf{A}, \mathbf{R})} \right) \\
& + \lambda \frac{\mathbf{u}_k^\top \mathbf{W} \mathbf{u}_m}{d_{km}(\mathbf{A}, \mathbf{R})} \left(p_k + p_m - 2 - \frac{((p_k - 1)(r_{km} - r_{kk}) + (p_m - 1)(r_{km} - r_{mm}))^2}{d_{km}^2(\mathbf{A}, \mathbf{R})} \right) \\
\frac{\partial^2 L_{\text{cpath}}(a_{kk}, \mathbf{r}_k, r_{kk})}{\partial r_{km} \partial r_{km'}} & = - \lambda \sum_{\substack{\ell=1 \\ \ell \notin \{k,m,m'\}}}^K \frac{\mathbf{u}_k^\top \mathbf{W} \mathbf{u}_\ell}{d_{k\ell}^3(\mathbf{A}, \mathbf{R})} p_m p_{m'} (r_{km} - r_{m\ell})(r_{km'} - r_{m'\ell}) \\
& - \lambda \frac{\mathbf{u}_k^\top \mathbf{W} \mathbf{u}_{m'}}{d_{km'}^3(\mathbf{A}, \mathbf{R})} ((p_k - 1)(r_{km'} - r_{kk}) + (p_m - 1)(r_{km'} - r_{m'm'})) p_m (r_{km} - r_{mm'}) \\
& + \lambda p_k \frac{\mathbf{u}_m^\top \mathbf{W} \mathbf{u}_{m'}}{d_{mm'}(\mathbf{A}, \mathbf{R})} \left(1 - \frac{p_k (r_{km'} - r_{km})^2}{d_{mm'}^2(\mathbf{A}, \mathbf{R})} \right) \\
& - \lambda \frac{\mathbf{u}_k^\top \mathbf{W} \mathbf{u}_m}{d_{km}(\mathbf{A}, \mathbf{R})} p_{m'} (r_{km'} - r_{mm'}) ((p_k - 1)(r_{km} - r_{kk}) + (p_m - 1)(r_{km} - r_{mm})) \\
\frac{\partial^2 L_{\text{cpath}}(a_{kk}, \mathbf{r}_k, r_{kk})}{\partial r_{km} \partial r_{kk}} & = - \lambda \sum_{\substack{\ell=1 \\ \ell \notin \{k,m\}}}^K \frac{\mathbf{u}_k^\top \mathbf{W} \mathbf{u}_\ell}{d_{k\ell}^3(\mathbf{A}, \mathbf{R})} p_m (p_k - 1)(r_{kk} - r_{k\ell})(r_{km} - r_{m\ell}) \\
& - \lambda (p_k - 1) \frac{\mathbf{u}_k^\top \mathbf{W} \mathbf{u}_m}{d_{km}(\mathbf{A}, \mathbf{R})} \left(1 - \frac{(p_k - 1)(r_{km} - r_{kk})}{d_{km}^2(\mathbf{A}, \mathbf{R})} (r_{km} - r_{kk}) \right) \\
& + \frac{(p_m - 1)(r_{km} - r_{mm})}{d_{km}^2(\mathbf{A}, \mathbf{R})} (r_{km} - r_{kk}) \\
\frac{\partial^2 L_{\text{cpath}}(a_{kk}, \mathbf{r}_k, r_{kk})}{\partial r_{kk}^2} & = \lambda (p_k - 1) \sum_{\substack{\ell=1 \\ \ell \neq k}}^K \mathbf{u}_k^\top \mathbf{W} \mathbf{u}_\ell \left(\frac{1}{d_{k\ell}(\mathbf{A}, \mathbf{R})} - \frac{(p_k - 1)(r_{kk} - r_{k\ell})^2}{d_{k\ell}^3(\mathbf{A}, \mathbf{R})} \right),
\end{aligned}$$

where the terms relating to $L_{\text{cov}}(a_{kk}, \mathbf{r}_k, r_{kk})$ are left out as they evaluate to zero. It should be noted that if the size of the k^{th} cluster is one, the variable r_{kk} is effectively not a part of the objective function. Consequently, the k^{th} element of the gradient is zero and the k^{th} row and column of the Hessian are also filled with zeros.

C Additional Simulation Results

This appendix provides supplementary simulation results from the experiments discussed in Section 3. Figure 10 illustrates the results for the chain simulation design with varying numbers of variables. Figure 11 shows the results for designs featuring an approximate block structure. The performance of the methods is evaluated based on estimation accuracy (Frobenius norm) and clustering quality (number of clusters and ARI).

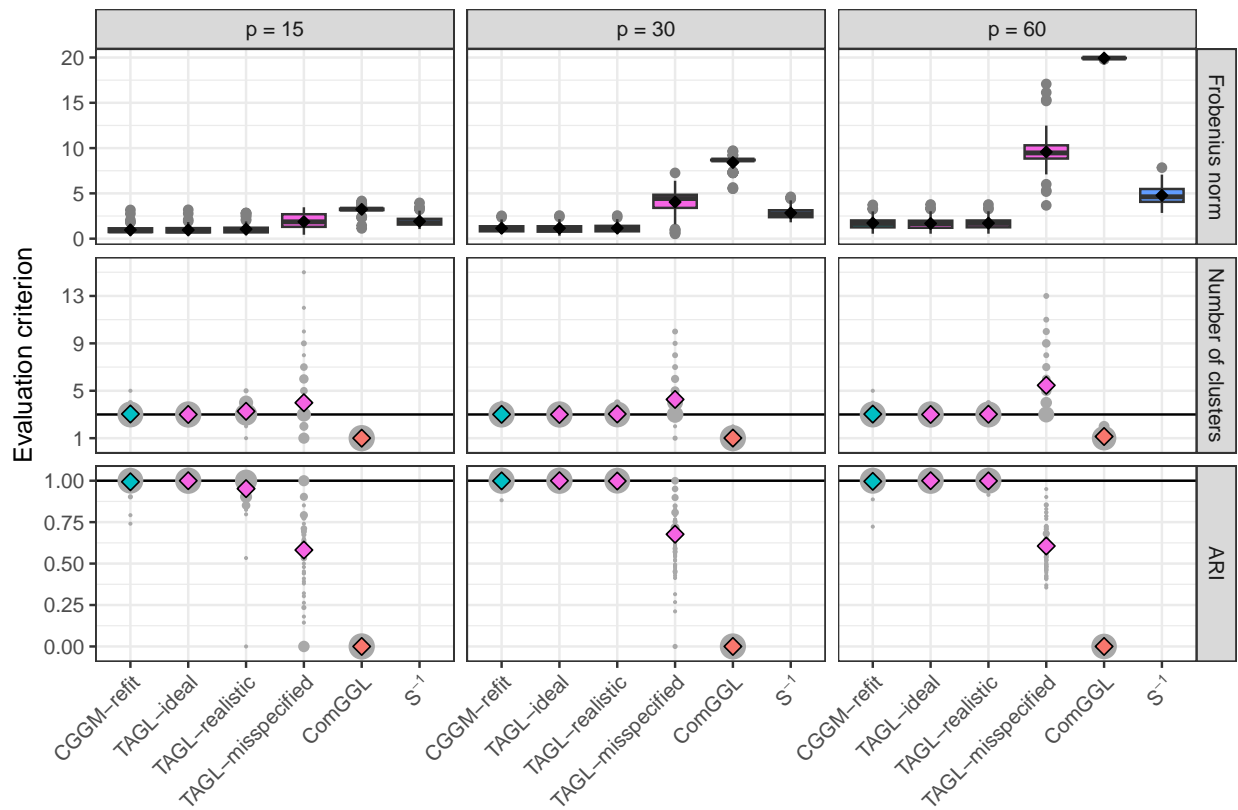


Figure 10: Results for the chain simulation design with an increasing number of variables (in separate columns). The top row contains boxplots of the Frobenius norm together with black diamonds representing the average. In the middle and bottom rows, diamonds display the average of the estimated number of clusters and the average ARI, respectively. In addition, the size of the grey dots represent the frequency of different values across the replications. Reference lines are drawn for the true number of clusters and the maximum possible ARI value. Aggregation performance is omitted for \mathbf{S}^{-1} as it does not perform any aggregation.

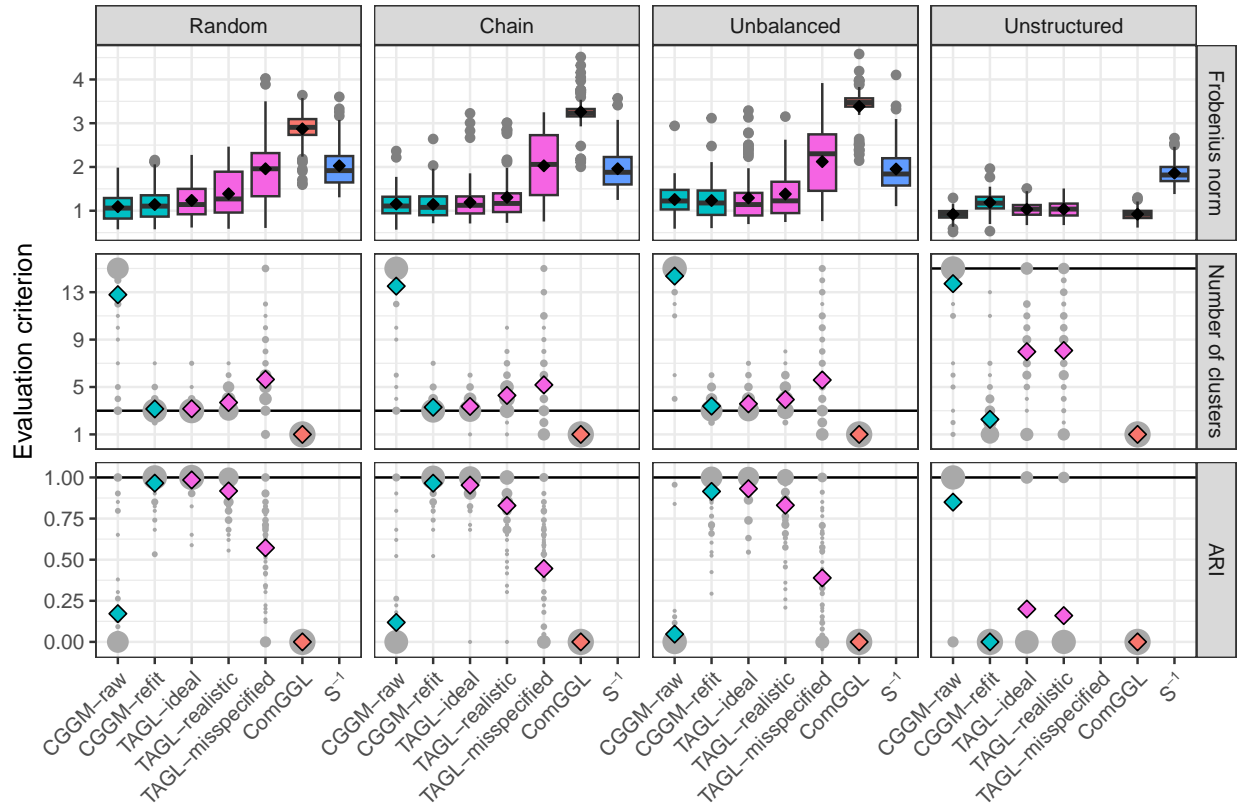


Figure 11: Results for the simulation designs with an approximate block structure (in separate columns). The top row contains boxplots of the Frobenius norm together with black diamonds representing the average. In the middle and bottom rows, diamonds display the average of the estimated number of clusters and the average ARI, respectively. In addition, the size of the grey dots represent the frequency of different values across the replications. Reference lines are drawn for the true number of clusters and the maximum possible ARI value. Aggregation performance is omitted for \mathbf{S}^{-1} as it does not perform any aggregation. In the unstructured design, a misspecified tree for TAGL does not exist since any tree hierarchy contains the true clustering (each variable being its own cluster).

D Humor Styles Questionnaire

This appendix contains information on the HSQ developed by Martin et al. (2003), which is analyzed in Section 5.3. The $p = 32$ items of the HSQ, grouped by the humor style being measured, are listed in Table 2 together with their position in the survey.

Humor style	Items
Affiliative	1. I usually don't laugh or joke around much with other people.* 5. I don't have to work very hard at making other people laugh—I seem to be a naturally humorous person. 9. I rarely make other people laugh by telling funny stories about myself.* 13. I laugh and joke a lot with my closest friends. 17. I usually don't like to tell jokes or amuse people.* 21. I enjoy making people laugh. 25. I don't often joke around with my friends.* 29. I usually can't think of witty things to say when I'm with other people.*
Self-enhancing	2. If I am feeling depressed, I can usually cheer myself up with humor. 6. Even when I'm by myself, I'm often amused by the absurdities of life. 10. If I am feeling upset or unhappy I usually try to think of something funny about the situation to make myself feel better. 14. My humorous outlook on life keeps me from getting overly upset or depressed about things. 18. If I'm by myself and I'm feeling unhappy, I make an effort to think of something funny to cheer myself up. 22. If I am feeling sad or upset, I usually lose my sense of humor.* 26. It is my experience that thinking about some amusing aspect of a situation is often a very effective way of coping with problems. 30. I don't need to be with other people to feel amused—I can usually find things to laugh about even when I'm by myself.
Aggressive	3. If someone makes a mistake, I will often tease them about it. 7. People are never offended or hurt by my sense of humor.* 11. When telling jokes or saying funny things, I am usually not very concerned about how other people are taking it. 15. I do not like it when people use humor as a way of criticizing or putting someone down.* 19. Sometimes I think of something that is so funny that I can't stop myself from saying it, even if it is not appropriate for the situation.

Table 2: List of the $p = 32$ items of the humor styles questionnaire of Martin et al. (2003), grouped by the humor style being measured and reported together with their position in the survey. Items marked with an asterisk are reverse-keyed, i.e., the responses on the five-point rating scale are reversed prior to analysis.

Table continues on the next page

Humor style	Items
	23. I never participate in laughing at others even if all my friends are doing it.*
	27. If I don't like someone, I often use humor or teasing to put them down.
	31. Even if something is really funny to me, I will not laugh or joke about it if someone will be offended.*
Self-defeating	4. I let people laugh at me or make fun at my expense more than I should.
	8. I will often get carried away in putting myself down if it makes my family or friends laugh.
	12. I often try to make people like or accept me more by saying something funny about my own weaknesses, blunders, or faults.
	16. I don't often say funny things to put myself down.*
	20. I often go overboard in putting myself down when I am making jokes or trying to be funny.
	24. When I am with friends or family, I often seem to be the one that other people make fun of or joke about.
	28. If I am having problems or feeling unhappy, I often cover it up by joking around, so that even my closest friends don't know how I really feel.
	32. Letting others laugh at me is my way of keeping my friends and family in good spirits.

Table 2: List of the $p = 32$ items of the humor styles questionnaire of Martin et al. (2003), grouped by the humor style being measured and reported together with their position in the survey. Items marked with an asterisk are reverse-keyed, i.e., the responses on the five-point rating scale are reversed prior to analysis.